Inorganic Chemistry

Article

[Mn₁₂O₁₂(OMe)₂(O₂CPh)₁₆(H₂O)₂]²⁻ Single-Molecule Magnets and Other Manganese Compounds from a Reductive Aggregation Procedure

Anastasios J. Tasiopoulos,[†,‡] Wolfgang Wernsdorfer,[#] Khalil A. Abboud,[†] and George Christou*,[†]

*Department of Chemistry, University of Florida, Gainesville, Florida 32611-7200, and
Laboratoire Louis Néel-CNRS, BP 166, 25 Avenue des Martyrs, 38042 Grenoble, Cedex 9, France*

A new synthetic procedure has been developed in Mn cluster chemistry involving reductive aggregation of permanganate (MnO₄⁻) ions in MeOH in the presence of benzoic acid, and the first products from its use are described. The reductive aggregation of NBuⁿ₄MnO₄ in MeOH/benzoic acid gave the new 4Mnᴵⱽ, 8Mnᴵᴵᴵ anion [Mn₁₂O₁₂(OMe)₂(O₂CPh)₁₆(H₂O)₂]²⁻, which was isolated as a mixture of two crystal forms (NBuⁿ₄)₂[Mn₁₂O₁₂(OMe)₂-(O₂CPh)₁₆(H₂O)₂]·2H₂O·4CH₂Cl₂ (**1a**) and (NBuⁿ₄)₂[Mn₁₂O₁₂(OMe)₂(O₂CPh)₁₆(H₂O)₂]·2H₂O·CH₂Cl₂ (**1b**). The anion of **1** contains a central [Mnᴵⱽ₄(μ₃-O)₂(μ-O)₂(μ-OMe)₂]⁶⁺ unit surrounded by a nonplanar ring of eight Mnᴵᴵᴵ atoms that are connected to the central Mn₄ unit by eight bridging μ₃-O²⁻ ions. This compound is very similar to the well-known [Mn₁₂O₁₂(O₂CR)₁₆(H₂O)₄] complexes (hereafter called "normal Mn₁₂"), with the main difference being the structure of the central cores. Longer reaction times (~2 weeks) led to isolation of polymeric [Mn(OMe)(O₂CPh)₂]ₙ (**2**), which contains a linear chain of repeating [Mnᴵᴵᴵ(μ-O₂CPh)₂(μ-OMe)Mnᴵᴵᴵ] units. The chains are parallel to each other and interact weakly through π-stacking between the benzoate rings. When KMnO₄ was used instead of NBuⁿ₄MnO₄, two types of compounds were obtained, [Mn₁₂O₁₂(O₂CPh)₁₆(H₂O)₄] (**3**), a normal Mn₁₂ complex, and [Mn₄O₂(O₂CPh)₈(MeOH)₄]·2MeOH (**4·2MeOH**), a new member of the Mn₄ butterfly family. The cyclic voltammogram of **1** exhibits three irreversible processes, two reductions and one oxidation. One-electron reduction of **1** by treatment with 1 equiv of I⁻ in CH₂Cl₂ gave (NBuⁿ₄)[Mn₁₂O₁₂(O₂CPh)₁₆(H₂O)₃]·6CH₂Cl₂ (**5·6CH₂Cl₂**), a normal Mn₁₂ complex in a one-electron reduced state. The variable-temperature magnetic properties of **1**, **2**, and **5** were studied by both direct current (dc) and alternating current (ac) magnetic susceptibility measurements. Variable-temperature dc magnetic susceptibility studies revealed that (i) complex **1** possesses an $S = 6$ ground state, (ii) complex **2** contains antiferromagnetically coupled chains, and (iii) complex **5** is a typical [Mn₁₂]⁻ cluster with an $S = 19/2$ ground state. Variable-temperature ac susceptibility measurements suggested that **5** and both isomeric forms of **1** (**1a,b**) are single-molecule magnets (SMMs). This was confirmed by the observation of hysteresis loops in magnetization vs dc field scans. In addition, **1a,b**, like normal Mn₁₂ clusters, display both faster and slower relaxing magnetization dynamics that are assigned to the presence of Jahn–Teller isomerism.

Introduction

An exciting development in the field of nanoscale magnetic materials occurred in 1993 when [Mn₁₂O₁₂(O₂CMe)₁₆-(H₂O)₄] (**6**) was identified as a nanoscale magnet,[1] the first to comprise discrete, (magnetically) noninteracting molecular units rather than a 3D extended lattice (metals, metal oxides, etc.). This discovery initiated the field of molecular nano-

magnetism, and such molecules have since been termed single-molecule magnets (SMMs).[2] Unlike traditional magnetic materials comprising metals, metal alloys, metal oxides, etc., SMMs do not derive their magnetic properties from interunit interactions and long-range ordering but from the intrinsic, intramolecular properties of individual molecules. Thus, each molecule is a single-domain magnetic particle,

* To whom correspondence should be addressed. E-mail: christou@chem.ufl.edu. Tel: +1-352-392-8314. Fax: +1-352-392-8757.
† University of Florida.
‡ Present address: Department of Chemistry, University of Cyprus, 1678 Nicosia, Cyprus.
# Laboratoire Louis Nèel.

(1) (a) Sessoli, R.; Tsai, H.-L.; Schake, A. R.; Wang, S.; Vincent, J. B.; Folting, K.; Gatteschi, D.; Christou, G.; Hendrickson, D. N. *J. Am. Chem. Soc.* **1993**, *115*, 1804. (b) Sessoli, R.; Gatteschi, D.; Caneschi, A.; Novak, M. A. *Nature* **1993**, *365*, 141.
(2) Aubin, S. M. J.; Wemple, M. W.; Adams, D. M.; Tsai, H.-L.; Christou, G.; Hendrickson, D. N. *J. Am. Chem. Soc.* **1996**, *118*, 7746.

and this is due to the combination of a large spin (S) and an Ising (easy-axis) magnetoanisotropy (negative zero-field splitting parameter, D), which results in a barrier to magnetization relaxation. The upper limit of the latter is given by $S^2|D|$ and $(S^2 - \frac{1}{4})|D|$ for integer and half-integer spin systems, respectively. Although several classes of homometallic and heterometallic SMMs are now known,[1-12] there

(3) (a) Christou, G.; Gatteschi, D.; Hendrickson, D. N.; Sessoli, R. *MRS Bull.* **2000**, *25*, 66. (b) Gatteschi, D.; Sessoli, R. *Angew. Chem., Int. Ed.* **2003**, *42*, 268.

(4) (a) Tasiopoulos, A. J.; Wernsdorfer, W.; Moulton, B.; Zaworotko, M. J.; Christou, G. *J. Am. Chem. Soc.* **2003**, *125*, 15274. (b) Tasiopoulos, A. J.; Vinslava, A.; Wernsdorfer, W.; Abboud, K. A.; Christou, G. *Angew. Chem., Int. Ed.* **2004**, *43*, 2117. (c) Price, D. J.; Batten, S. R.; Moubaraki, B.; Murray, K. S. *Chem. Commun.* **2002**, 762. (d) Aubin, S. M. J.; Dilley, N. R.; Pardi, L.; Krzystek, J.; Wemple, M. W.; Brunel, L.-C.; Maple, M. B.; Christou, G.; Hendrickson, D. N. *J. Am. Chem. Soc.* **1998**, *120*, 4991. (e) Brechin, E. K.; Soler, M.; Christou, G.; Helliwell, M.; Teat, S. J.; Wernsdorfer, W. *Chem. Commun.* **2003**, 1276. (f) Soler, M.; Wernsdorfer, W.; Folting, K.; Pink, M.; Christou, G. *J. Am. Chem. Soc.* **2004**, *126*, 2156. (g) Sanudo, E. C.; Wernsdorfer, W.; Abboud, K. A.; Christou, G. *Inorg. Chem.* **2004**, *43*, 4137. (h) Murugesu, M.; Raftery, J.; Wernsdorfer, W.; Christou, G.; Brechin, E. K. *Inorg. Chem.* **2004**, *43*, 4203.

(5) (a) Brechin, E. K.; Yoo, J.; Nakano, M.; Huffman, J. C.; Hendrickson, D. N.; Christou, G. *Chem. Commun.* **1999**, 783. (b) Yoo, J.; Brechin, E. K.; Yamaguchi, A.; Nakano, M.; Huffman, J. C.; Maniero, A. L.; Brunel, L.-C.; Awaga, K.; Ishimoto, H.; Christou, G.; Hendrickson, D. N. *Inorg. Chem.* **2000**, *39*, 3615. (c) Brechin, E. K.; Soler, M.; Davidson, J.; Hendrickson, D. N.; Parsons, S.; Christou, G. *Chem. Commun.* **2002**, 2252. (d) Jones, L. F.; Brechin, E. K.; Collison, D.; Harrison, A.; Teat, S. J.; Wernsdorfer, W. *Chem. Commun.* **2002**, 2974. (e) Moragues-Canovas, M.; Helliwell, M.; Ricard, L.; Riviere, E.; Wernsdorfer, W.; Brechin, E. K.; Mallah, T. *Eur. J. Inorg. Chem.* **2004**, 2219. (f) Milios, C. J.; Raptopoulou, C. P.; Terzis, A.; Lloret, F.; Vicente, R.; Perlepes, S. P.; Escuer, A. *Angew. Chem., Int. Ed.* **2004**, *43*, 210. (g) Boudalis, A. K.; Donnadieu, B.; Nastopoulos, V.; Clemente-Juan, J. M.; Mari, A.; Sanakis, Y.; Tuchagues, J.-P.; Perlepes, S. P. *Angew. Chem., Int. Ed.* **2004**, *43*, 2266. (h) Andres, H.; Basler, R.; Blake, A. J.; Cadiou, C.; Chaboussant, G.; Grant, C. M.; Güdel, H.-U.; Murrie, M.; Parsons, S.; Paulsen, C.; Semadini, F.; Villar, V.; Wernsdorfer, W.; Winpenny, R. E. P. *Chem.—Eur. J.* **2002**, *8*, 4867.

(6) (a) Aubin, S. M. J.; Sun, Z.; Guzei, I. A.; Rheingold, A. L.; Christou, G.; Hendrickson, D. N. *Chem. Commun.* **1997**, 2239. (b) Sun, Z.; Ruiz, D.; Rumberger, E.; Incarvito, C. D.; Folting, K.; Rheingold, A. L.; Christou, G.; Hendrickson, D. N. *Inorg. Chem.* **1998**, *37*, 4758. (c) Ruiz, D.; Sun, Z.; Albela, B.; Folting, K.; Ribas, J.; Christou, G.; Hendrickson, D. N. *Angew. Chem., Int. Ed.* **1998**, *37*, 300. (d) Sun, Z.; Ruiz, D.; Dilley, N. R.; Soler, M.; Ribas, J.; Folting, K.; Maple, M. B.; Christou, G.; Hendrickson, D. N. *Chem. Commun.* **1999**, 1973. (e) Aubin, S. M. J.; Sun, Z.; Eppley, H. J.; Rumberger, E. M.; Guzei, I. A.; Folting, K.; Gantzel, P. K.; Rheingold, A. L.; Christou, G.; Hendrickson, D. N. *Inorg. Chem.* **2001**, *40*, 2127. (f) Eppley, H. J.; Tsai, H.-L.; de Vries, N.; Folting, K.; Christou, G.; Hendrickson, D. N. *J. Am. Chem. Soc.* **1995**, *117*, 301. (g) Soler, M.; Wernsdorfer, W.; Sun, Z.; Huffman, J. C.; Hendrickson, D. N.; Christou, G. *Chem. Commun.* **2003**, 2672.

(7) Soler, M.; Artus, P.; Folting, K.; Huffman, J. C.; Hendrickson, D. N.; Christou, G. *Inorg. Chem.* **2001**, *40*, 4902.

(8) (a) Artus, P.; Boskovic, C.; Yoo, J.; Streib, W. E.; Brunel, L.-C.; Hendrickson, D. N.; Christou, G. *Inorg. Chem.* **2001**, *40*, 4199. (b) Boskovic, C.; Pink, M.; Huffman, J. C.; Hendrickson, D. N.; Christou, G. *J. Am. Chem. Soc.* **2001**, *123*, 9914. (c) Chakov, N. E.; Wernsdorfer, W.; Abboud, K. A.; Hendrickson, D. N.; Christou, G. *Dalton Trans.* **2003**, 2243.

(9) (a) Aubin, S. M. J.; Sun, Z.; Pardi, L.; Krzystek, J.; Folting, K.; Brunel, L.-C.; Rheingold, A. L.; Christou, G.; Hendrickson, D. N. *Inorg. Chem.* **1999**, *38*, 5329. (b) Kuroda-Sowa, T.; Lam, M.; Rheingold, A. L.; Frommen, C.; Reiff, W. M.; Nakano, M.; Yoo, J.; Maniero, A. L.; Brunel, L. -C.; Christou, G.; Hendrickson, D. N. *Inorg. Chem.* **2001**, *40*, 6469. (c) Chakov, N. E.; Soler, M.; Wernsdorfer, W.; Abboud, K. A.; Christou, G. *Inorg. Chem.* **2005**, in press.

(10) (a) Soler, M.; Chandra, S. K.; Ruiz, D.; Davidson, E. R.; Hendrickson, D. N.; Christou, G. *Chem. Commun.* **2000**, 2417. (b) Soler, M.; Wernsdorfer, W.; Abboud, K. A.; Huffman, J. C.; Davidson, E. R.; Hendrickson, D. N.; Christou, G. *J. Am. Chem. Soc.* **2003**, *125*, 3576.

is a continuing need for new types of such molecules to improve our understanding of this phenomenon. Two directions that we have been pursuing along these lines are (i) development of synthetic routes to new high-nuclearity metal complexes[4,5] and (ii) modifications of known SMMs in a controlled fashion.[6-10] The best and most thoroughly studied SMMs to date are members of the $[Mn_{12}O_{12}(O_2CR)_{16}(H_2O)_4]$ (Mn_{12}) family with $S = 10$. A number of such Mn_{12} derivatives have been prepared in their neutral,[1,6-8] one-electron reduced,[6f,9] or two-electron[10] reduced versions with a variety of carboxylate,[6,9,10] mixed carboxylate,[7] and mixed carboxylate/non-carboxylate[8] ligands. In all such modifications, the $[Mn_{12}(\mu_3\text{-O})_{12}]$ core remains essentially the same.

We describe several new results in this work, and a unifying theme among them is that they all arise directly or indirectly from the use of a new synthetic procedure in Mn chemistry that we have recently developed. This has allowed synthetic entry into a new class of polynuclear Mn carboxylate species. We refer to this procedure as "reductive aggregation", in which the high oxidation state, mononuclear permanganate (MnO_4^-) ion is reduced by MeOH in the presence of excess carboxylic acid. We describe three types of compounds that have been obtained with this synthetic procedure: $(NBu^n_4)_2[Mn_{12}O_{12}(OMe)_2(O_2CPh)_{16}(H_2O)_2]$ (**1**) salts containing a new type of anion that is a structural derivative of the normal Mn_{12} complexes; the chain polymer $[Mn(OMe)(O_2CPh)_2]_n$ (**2**); the cluster $[Mn_4O_2(O_2CPh)_8(MeOH)_4]$ (**4**). We have also recently reported elsewhere an additional family of Mn_{16} clusters obtained by reductive aggregation.[11] Attempted reduction of **1** led to the isolation of $(NBu^n_4)[Mn_{12}O_{12}(O_2CPh)_{16}(H_2O)_3]$ (**5**). We herein describe the syntheses, structures, and properties of complexes **1**, **2**, **4**, and **5**, which have established that the anion of **1** is a new addition to the family of SMMs. Portions of this work have been previously communicated.[12]

Experimental Section

Syntheses. All manipulations were performed under aerobic conditions with the use of materials as received unless otherwise indicated; water was distilled in-house. $NBu^n_4MnO_4$ was prepared by a literature procedure.[13] ***Warning***: *Appropriate care should be taken in the use of $NBu^n_4MnO_4$, and readers are referred to the detailed warning given elsewhere.*[14] Elemental analyses were performed by the in-house facilities of the Chemistry Department, University of Florida.

$(NBu^n_4)_2[Mn_{12}O_{12}(O_2CPh)_{16}(OMe)_2(H_2O)_2]$ (1). Freshly prepared $NBu^n_4MnO_4$ (1.0 g, 2.8 mmol) was added in small portions to a solution of benzoic acid (5.0 g, 41 mmol) in MeOH (15 mL), and the mixture was stirred for ~5 min. The resulting purple solution was left undisturbed at room temperature overnight. During this time, the color slowly turned dark brown, and black crystals slowly formed. The latter, which were found to be poor diffractors of X-rays, were collected by filtration, washed with MeOH (2 ×

(11) King, P.; Wernsdorfer, W.; Abboud, K. A.; Christou, G. *Inorg. Chem.* **2004**, *43*, 7315.

(12) Tasiopoulos, A. J.; Wernsdorfer, W.; Abboud, K. A.; Christou, G. *Angew. Chem., Int. Ed.* **2004**, *43*, 6338.

(13) Sala, T.; Sargent, M. V. *Chem. Commoun.* **1978**, 253.

(14) Vincent, J. B.; Folting, K.; Huffman, J. C.; Christou, G. *Inorg. Chem.* **1986**, *25*, 996.

10 mL), and dried in vacuo. The material was recrystallized from CH_2Cl_2/hexanes to give a mixture of diamond-shaped crystals of **1**·$2H_2O$·$4CH_2Cl_2$ (**1a**) and needle-shaped crystals of **1**·$2H_2O$·CH_2Cl_2 (**1b**), identified crystallographically, in an overall combined yield of 0.12 g (15% based on Mn). These were collected by filtration, washed with hexanes, and dried in vacuo. Both **1a,b** were good diffractors of X-rays, as long as they were kept in contact with the mother liquor to prevent solvent loss. Anal. Calcd (found) for **1**·$2H_2O$: C, 51.45 (51.26); H, 4.91 (4.72); N, 0.82 (0.70). Selected IR data (KBr, cm^{-1}): 3430 (s, br), 3065 (w) 2965 (w), 2925 (w), 2875 (w), 1598 (s), 1560 (s), 1532 (s), 1492 (m), 1448 (m), 1417 (s), 1306 (w), 1177 (m), 1069 (w), 1026 (m), 838 (w), 718 (s), 675 (s), 625 (m, br), 499 (m).

[Mn(OMe)(O₂CPh)₂]ₙ (2). The previous procedure was followed except that the reaction solution was allowed to stand at room temperature for an extended period of ∼2 weeks. During this time, the crystals of complex **1** that formed redissolved and were replaced by dark crystals of complex **2**. These were collected by filtration, washed with MeOH (2 × 10 mL), and dried in vacuo. The yield was 70%. Anal. Calcd (found) for **2**: C, 54.90 (54.67); H: 3.99 (3.83). Selected IR data (KBr, cm^{-1}): 3421 (m, br), 3065 (m), 3023 (w), 2940 (w), 1693 (m), 1592 (s), 1552 (s), 1491 (m), 1448 (m), 1386 (s), 1306 (m), 1177 (m), 1159 (w), 1143 (w), 1069 (m), 1026 (m), 992 (m), 937 (w), 841 (w), 816 (w), 716 (s), 683 (m), 610 (m), 558 (m), 483 (m).

[Mn₁₂O₁₂(O₂CPh)₁₆(H₂O)₄] (3). Method A. Solid $KMnO_4$ (1.0 g, 6.3 mmol) was added in small portions to a solution of benzoic acid (5.0 g, 41 mmol) in MeOH (15 mL), and the mixture was stirred for ∼2 h. During this time, the $KMnO_4$ slowly dissolved and a dark brown precipitate formed. The precipitate was collected by filtration, washed with MeOH and Et_2O, and recrystallized from CH_2Cl_2/hexanes to give black crystals of **3** in 40% overall yield. The identity of the product was confirmed by elemental analysis and IR spectral comparison with an authentic sample.[1a] Anal. Calcd (found) for **3**: C, 47.02 (47.12); H: 3.10 (3.20). Selected IR data (KBr, cm^{-1}): 3420 (m, br), 3065 (w), 1598 (s), 1560 (s), 1522 (s), 1492 (m), 1448 (m), 1418 (s), 1350 (m), 1308 (w), 1178 (m), 1155 (w), 1140 (w), 1068 (w), 1026 (m), 934 (w), 839 (w), 718 (s), 677 (s), 654 (m), 615 (m), 550 (m), 514 (m).

Method B. The reaction procedure to complex **1** was followed except that the reaction solution was allowed to stand at room temperature for 48 h. The black crystals that were present after this time were collected by filtration, washed with MeCN (2 × 10 mL) to remove traces of complex **1** and then Et_2O (10 mL), and dried in vacuo. The product was identified by IR spectral comparison with authentic material. The yield was 30%.

Method C. Method B was repeated using EtOH in place of MeOH. Black crystals were again obtained and collected as in method B. The yield was 30%. The product was identified by IR spectral comparison with authentic material.

Method D. Complex **1**·$2H_2O$ (0.1 g, 0.03 mmol) were dissolved in MeCN (6 mL), and the solution was left to slowly evaporate at room temperature. Black crystals slowly formed, and these were collected by filtration and recrystallized from CH_2Cl_2/hexanes to give **3** in 70% yield. The product was identified by IR spectral comparison with authentic material.

[Mn₄O₂(O₂CPh)₈(MeOH)₄] (4). Solid $KMnO_4$ (1.0 g, 6.3 mmol) was added in small portions to a solution of benzoic acid (5.0 g, 41 mmol) in MeOH (15 mL), and the mixture was stirred for ∼20 min. During this time, the $KMnO_4$ slowly dissolved and a dark brown precipitate formed. The solution was filtered and the filtrate allowed to stand undisturbed at room temperature. After 2 days, dark red X-ray-quality crystals of **4**·$2MeOH$ had formed. The yield

was 10%. Anal. Calcd (found) for **4**·H_2O: C, 47.02 (47.12); H: 3.10 (3.20). Selected IR data (KBr, cm^{-1}): 3400 (m, br), 3065 (m), 1600 (s), 1560 (s), 1520 (s), 1491 (m), 1448 (m), 1399 (s), 1307 (w), 1177 (m), 1157 (w), 1143 (w), 1070 (m), 1026 (m), 1002 (w), 938 (w), 839 (w), 816 (w), 717 (s), 678 (s), 648 (m), 616 (m), 508 (w), 478 (w)

(NBuⁿ₄)[Mn₁₂O₁₂(O₂CPh)₁₆(H₂O)₃] (5). To a solution of complex **1**·$2H_2O$ (0.500 g 0.147 mmol) in CH_2Cl_2 (60 mL) was added NBu^n_4I (54.3 mg, 0.147 mmol), and the mixture was stirred overnight at room temperature. The solvent was removed in vacuo, and the residue washed with hexanes (6 × 60 mL) until the washings were colorless and then washed with Et_2O (3 × 20 mL) and dried in vacuo. Recrystallization of the solid from CH_2Cl_2/hexanes gave large needles of **5**·$6CH_2Cl_2$, suitable for X-ray crystallography. The crystals were collected by filtration, washed with hexanes, and dried in vacuo. The overall yield was 60%. Anal. Calcd (found) for **5**·H_2O: C, 49.54 (49.35); H, 4.03 (3.91); N, 0.82 (0.75). Selected IR data (KBr, cm^{-1}): 3445 (m, br), 3064 (w), 2962 (m), 2932 (w), 2875 (w), 1598 (s), 1560 (s), 1537 (m), 1491 (w), 1472 (w), 1448 (m), 1418 (s), 1391 (s), 1303 (w), 1257 (w), 1176 (m), 1140 (w), 1069 (w), 1026 (m), 938 (w), 882 (w), 839 (w), 720 (s), 676 (s), 655 (m), 616 (m), 507 (m).

X-ray Crystallogrphy. Data for complexes **1a**, **1b**, **2**, **4**·$2MeOH$, and **5**·$6CH_2Cl_2$ were collected at 173 K on a Siemens SMART PLATFORM equipped with a CCD area detector and a graphite monochromator utilizing Mo Kα radiation (λ = 0.710 73 Å). Cell parameters were refined using up to 8192 reflections. A full sphere of data (1850 frames) was collected using the ω-scan method (0.3° frame width). The first 50 frames were remeasured at the end of data collection to monitor instrument and crystal stability (maximum correction on I was < 1%). Absorption corrections by integration were applied on the basis of measured indexed crystal faces. The structures were solved by the Direct Methods in SHELXTL6[15] and refined using full-matrix least squares. The non-hydrogen atoms were refined anisotropically, whereas the hydrogen atoms were placed in calculated positions and refined as riding on their respective carbon atoms.

For complex **1a**, the asymmetric unit consists of half the Mn_{12} anion, a $NBu^n_4{}^+$ cation, and two CH_2Cl_2 and one H_2O molecules of crystallization. The CH_2Cl_2 molecules were disordered and could not be modeled properly; thus, program SQUEEZE, a part of the PLATON package of crystallographic software, was used to calculate the solvent disorder area and remove its contribution to the overall intensity data.[16] A total of 946 parameters were refined in the final cycles of refinement on F^2.

For complex **1b**, the asymmetric unit consists of half the Mn_{12} anion, two-half $NBu^n_4{}^+$ cations disordered about inversion centers, and half a CH_2Cl_2 molecule. The latter was disordered and could not be modeled properly; thus, program SQUEEZE, a part of the PLATON package of crystallographic software, was used to calculate the solvent disorder area and remove its contribution to the overall intensity data.[16] The phenyl rings containing C1, C9, and C16 were disordered, and each was refined as an ideal hexagonal rigid group. They were refined in two parts with their occupation factors dependently refined. The benzoate group containing C30 and a water molecule are disordered between three adjacent Mn centers, the benzoate bridging the first and central Mn, or the central and third Mn, with the water occupying the

(15) Sheldrick, G. M. *SHELXTL6*; Bruker-AXS: Madison, WI, 2000.
(16) (a) PLATON: Spek, A. L. *Acta Crystallogr., Sect. A* **1990**, *46*, C34. (b) SQUEEZE: van der Sluis, P.; Spek, A. L. *Acta Crystallogr., Sect. A* **1990**, *46*, 194−201.

remaining site. A total of 953 parameters were refined in the final cycles of refinement on F^2.

The structure of complex **2** consists of parallel chains that contain two crystallographically independent Mn ions linked by one methoxide and two benzoate ligands. A total of 194 parameters were refined in the final cycles of refinement on F^2. No disorder problems were encountered, a situation that benefited from the absence of solvent molecules of crystallization.

For complex **4·2MeOH**, the asymmetric unit consists of half a Mn₄ cluster and one MeOH molecule of crystallization. The H atoms of all the MeOH molecules were located from a difference Fourier map phased on the non-hydrogen atoms and refined freely. A total of 422 parameters were refined in the final cycles of refinement on F^2.

For complex **5·6CH₂Cl₂**, the asymmetric unit contains the complete $[Mn_{12}]^-$ anion, a $NBu^n_4{}^+$ cation, and six CH₂Cl₂ solvent molecules. The solvent molecules were disordered and could not be modeled properly; thus, program SQUEEZE, a part of the PLATON package of crystallographic software, was used to calculate the solvent disorder area and remove its contribution to the overall intensity data.[16] The cluster has three coordinated water molecules, and their six H atoms were located in a difference Fourier map; five of them were refined freely and the last was placed in a riding model. A total of 1706 parameters were refined in the final cycles of refinement on F^2.

Other Studies. Infrared spectra were recorded in the solid state (KBr pellets) using a Nicolet model Nexus 670 FTIR spectrometer in the 400−4000 cm⁻¹ range. Cyclic voltammetry was performed on ∼1.0 mM solutions at a 100 mV/s scan rate with a BAS CV-50W voltammetric analyzer and a standard three-electrode assembly (glassy-carbon working electrode, Pt wire auxiliary electrode, Ag/AgNO₃ reference electrode), with 0.1 M $NBu^n_4PF_6$ as supporting electrolyte. Potentials are quoted versus the ferrocene/ferrocenium couple under the same conditions. Variable-temperature dc and ac magnetic susceptibility data were collected at the University of Florida using a Quantum Design MPMS-XL SQUID magnetometer equipped with a 7 T (70 kG) magnet and operating in the 1.8−300 K range. Samples were embedded in solid eicosane to prevent torquing. Magnetization versus field and temperature data were fit using the program MAGNET.[17] A diamagnetic correction to the observed susceptibilities was applied using Pascal's constants. Studies at ultralow temperatures (<1.8 K) were performed on single crystals at Grenoble using an array of micro-SQUIDs.[18] The high sensitivity of this magnetometer allows the study of single crystals of SMMs of the order of 10−500 μm; the field can be applied in any direction by separately driving three orthogonal coils.

Results and Discussion

Syntheses. One of the many synthetic strategies that we have employed in the past for the synthesis of high oxidation state Mn$_x$ clusters has been the comproportionation reaction between a Mn²⁺ source and MnO_4^- (i.e. Mn^{VII}) in the presence of carboxylate and/or chelating groups. For example, the 4:1 ratio, respectively, of such reagents leads to an average oxidation state in solution of Mn^{III} (eq 1), allowing

$$4Mn^{2+} + Mn^{7+} \rightarrow 5Mn^{3+} \qquad (1)$$

subsequent isolation of cluster products at this oxidation level, such as the $[Mn_4O_2(O_2CR)_7(L-L)_2]^z$ butterfly-like

complexes, where L−L is a chelating ligand such as picolinate.[19] Recently, we modified this comproportionation reaction by using Ce^{IV} as the oxidizing agent in place of MnO_4^-, and this led to a family of new Mn/Ce clusters containing various Mn:Ce ratios.[20]

The synthesis of the normal Mn₁₂ compound $[Mn_{12}O_{12}(O_2CMe)_{16}(H_2O)_4]$ is also a comproportionation reaction, between Mn(O₂CMe)₂·4H₂O and KMnO₄ in 60% aqueous acetic acid, but with a higher proportion of MnO_4^- than eq 1 to give the higher average Mn oxidation state of Mn$^{3.33+}$ in this cluster.[21] When this reaction was instead carried out in MeOH/acetic acid, a number of products were isolated, depending on the ratios of the reactants, including Mn₁₆ and Mn₈₄ clusters.[4b,c] The present work represents an extension of this investigation, namely to explore what would happen if we omit the Mn^{II} component of the comproportionation and allow the MeOH to act as the reductant of the MnO_4^-. The hope was that new high oxidation state Mn clusters would result as the MnO_4^- was progressively reduced and aggregation occurred, with the MeOH potentially also providing methoxide bridging ligands. The excess of carboxylic acid provides an acidic environment that prevents precipitation of Mn oxides and/or hydroxides and also provides a source of carboxylate ligands. This approach, which we refer to as "reductive aggregation" of MnO_4^-, has indeed fulfilled our expectations and proven a useful route to new species.

Most of the results in this work were obtained from a MeOH/PhCO₂H medium. Thus, dissolution of $NBu^n_4MnO_4$ in a methanolic solution of benzoic acid at room temperature gave a purple solution which slowly turned dark brown, and overnight storage of this solution undisturbed gave a black crystalline product. These crystals were poor diffractors of X-rays. Recrystallization from CH₂Cl₂/hexanes gave two types of black crystals, diamonds and needles, in a total yield of 15%. These were crystallographically characterized as **1·2H₂O·4CH₂Cl₂** and **1·2H₂O·CH₂Cl₂**, respectively, both containing the same anion $[Mn_{12}O_{12}(OMe)_2(O_2CPh)_{16}(H_2O)_2]^{2-}$ ($[Mn_{12}']^{2-}$; 4Mn^{IV}, 8Mn^{III}) with an average Mn oxidation state of +3.33. Its formation is summarized in eq 2, where the electrons are coming from the oxidation of MeOH to HCHO and/or HCO₂H and the protons from the excess of PhCO₂H present.

$$12MnO_4^- + 16PhCO_2H + 2MeOH + 44e^- + 54H^+ \rightarrow$$
$$[Mn_{12}O_{12}(OMe)_2(O_2CPh)_{16}(H_2O)_2]^{2-} + 34H_2O \quad (2)$$
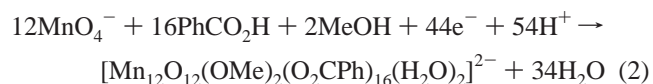
When the purple reaction solution was instead maintained undisturbed at room temperature for ∼48 h, the crystals that were obtained in 40% yield were instead $[Mn_{12}O_{12}(O_2CPh)_{16}(H_2O)_4]$ (**3**; 4Mn^{IV}, 8Mn^{III}), a known member of the normal

(17) Davidson, E. R. *MAGNET*; Indiana University: Bloomington, IN, 1999.

(18) Wernsdorfer, W. *Adv. Chem. Phys.* **2001**, *118*, 99.

(19) Libby, E.; McCusker, J. K.; Schmitt, E. A.; Folting, K.; Hendrickson, D. N.; Christou, G. *Inorg. Chem.* **1991**, *30*, 3486.

(20) (a) Tasiopoulos, A. J.; O'Brien, T. A.; Abboud, K. A.; Christou, G. *Angew. Chem., Int. Ed.* **2004**, *43*, 345. (b) Bhaduri, S.; Tasiopoulos, A. J.; Bolcar, M. A.; Abboud, K. A.; Streib, W. E.; Christou, G. *Inorg. Chem.* **2003**, *42*, 1483.

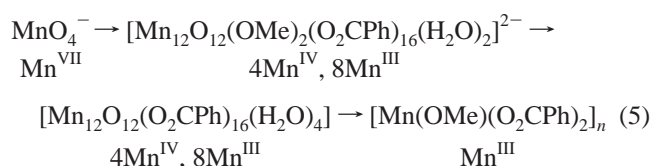(21) Lis, T. *Acta Crystallogr., Sect. B* **1980**, *B36*, 2042.

Mn_{12} family with an average Mn oxidation state of $+3.33$. Any remaining traces of complex **1** were removed by washing the crystals with MeCN. The formation of **3** is summarized in eq 3.

$$12MnO_4^- + 16PhCO_2H + 44e^- + 56H^+ \rightarrow$$
$$[Mn_{12}O_{12}(O_2CPh)_{16}(H_2O)_4] + 32H_2O \quad (3)$$
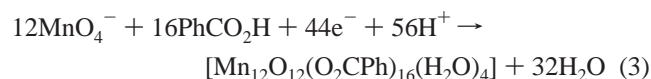
When the storage time at room temperature of the initially purple solution was extended to 2 or more weeks, dark brown crystals of $[Mn(OMe)(O_2CPh)_2]_n$ (**2**; Mn^{III}) were now obtained in 70% yield. Solutions that were stored for longer periods, up to a few months, also gave compound **2**, which thus seems to the terminal point of this reaction, under these conditions at least, probably primarily due to its high insolubility and relatively low oxidation state of Mn^{III}, which prevent further reduction by the MeOH. Its formation is summarized in eq 4.

$$nMnO_4^- + 2nPhCO_2H + nMeOH + 4ne^- + 5nH^+ \rightarrow$$
$$[Mn(OMe)(O_2CPh)_2]_n + 4nH_2O \quad (4)$$
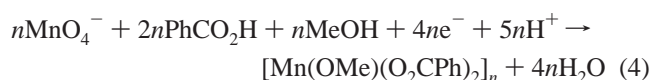
The identity of the isolated products indicates the formation of progressively lower oxidation state products as the reaction times are extended and the average Mn oxidation state in solution progressively decrease due to reduction by MeOH. Complex **1** is only obtained in low yield (15%), consistent with the relative instability of this complex, which readily converts to **3** (vide infra). Although other species are undoubtedly formed as the MnO_4^- is progressively reduced, **1** is the first one that we have been able to identify by isolation, and even this readily reacts further to give **3**; dissolution of $[Mn_{12}O_{12}(O_2CR)_{16}(H_2O)_4]$ compounds in MeOH does not give the analogue of **1**, and we are thus confident that the sequence of species formation in the reductive aggregation is **1** and then **3**. Longer reaction times then cause slow dissolution of **3** to give complex **2**, a Mn^{III} compound, consistent with further reduction of the average Mn oxidation state in solution by further reduction of remaining Mn^{IV} in solution and in the crystals of **3** to Mn^{III}. This overall sequence is summarized in eq 5. When the reaction was performed in EtOH, crystals of complex **3** were obtained when the solution was left undisturbed at room temperature for $\sim$ 48 h.
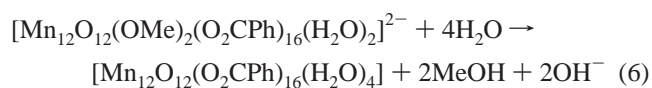
$$\underset{Mn^{VII}}{MnO_4^-} \rightarrow \underset{4Mn^{IV},\ 8Mn^{III}}{[Mn_{12}O_{12}(OMe)_2(O_2CPh)_{16}(H_2O)_2]^{2-}} \rightarrow$$

$$\underset{4Mn^{IV},\ 8Mn^{III}}{[Mn_{12}O_{12}(O_2CPh)_{16}(H_2O)_4]} \rightarrow \underset{Mn^{III}}{[Mn(OMe)(O_2CPh)_2]_n} \quad (5)$$

The permanganate salt employed is crucial. When solid $KMnO_4$ was used, it of course dissolved much more slowly in $MeOH/PhCO_2H$ than $NBu^n_4MnO_4$, and during this time a brown precipitate continuously formed from the stirring solution. After 2 h, with undissolved $KMnO_4$ still present, the precipitate was isolated by filtration and recrystallized from CH_2Cl_2/hexanes, and the resulting crystals were

identified as complex **3**. When the solution was filtered after stirring for only $\sim$20 min and the brown filtrate maintained at room temperature for 48 h, red crystals of $[Mn_4O_2(O_2CPh)_8(MeOH)_4]\cdot2MeOH$ (**4**; $4Mn^{III}$) were formed.

It is clear that the overall reactions are very complicated, and the reaction solution likely contains a complicated mixture of several species in equilibrium, with factors such as relative solubility, lattice energies, crystallization kinetics, and others determining the identity of the isolated product. One (or more) of these factors is undoubtedly the reason that by changing the solvent from MeOH to EtOH or the carboxylic acid used from benzoic to phenylacetic, chloroacetic, and bromoacetic acids, a variety of different products were formed. The latter refers to work published elsewhere that reported that the use of the indicated carboxylic acids in place of benzoic acid leads to the formation of Mn_{16} products.[11]

Complex **1** converts to normal Mn_{12} complex **3** on dissolution in MeCN followed by slow evaporation at room temperature, which gave black crystals of **3** in 70% yield. This is perhaps not surprising given that this conversion merely requires the loss of two MeO^- groups, which is probably triggered by water in the solvent, as summarized in eq 6. A similar conversion was probably responsible for

$$[Mn_{12}O_{12}(OMe)_2(O_2CPh)_{16}(H_2O)_2]^{2-} + 4H_2O \rightarrow$$
$$[Mn_{12}O_{12}(O_2CPh)_{16}(H_2O)_4] + 2MeOH + 2OH^- \quad (6)$$

the observation of two irreversible reduction processes when a fresh solution of **1** was studied by cyclic voltammetry in CH_2Cl_2. This is in contrast to normal Mn_{12} complex **3**, which shows two reversible reductions and one oxidation. We nevertheless carried out the one-electron reduction of **1** in CH_2Cl_2 with 1 equiv of NBu^n_4I using our previously developed procedure,[6f,9a,10] and the product after workup was $(NBu^n_4)[Mn_{12}O_{12}(O_2CPh)_{16}(H_2O)_3]$ (**5**), the one-electron-reduced version of the normal Mn_{12} species.

Description of Structures. Crystallographic data collection and structure refinement details for **1a**, **1b**, **2**, **4**·2MeOH, and **5**·$6CH_2Cl_2$ are summarized in Table 1. A labeled PovRay representation of the anion of **1** is shown in Figure 1. Selected interatomic distances for **1a,b** are listed in Tables 2 and 3, respectively. Complex **1** crystallizes as a mixture of diamond-like (**1a**) and needlelike (**1b**) crystals, both of which were crystallographically characterized and found to be **1**·$2H_2O$·$4CH_2Cl_2$ (**1a**) and **1**·$2H_2O$·CH_2Cl_2 (**1b**). Both contain the same $[Mn_{12}O_{12}(OMe)_2(O_2CPh)_{16}(H_2O)_2]^{2-}$ dianion, abbreviated $[Mn_{12}']^{2-}$. Complex **1a** crystallizes in the orthorhombic space group *Pbca* with the $[Mn_{12}']^{2-}$ cluster lying on a center of symmetry. The $[Mn_{12}']^{2-}$ anion (Figure 1) contains a central $[Mn^{IV}_4(\mu_3\text{-}O)_2(\mu\text{-}O)_2(\mu\text{-}OMe)_2]^{6+}$ core, surrounded by a nonplanar ring of eight near-octahedral Mn^{III} atoms that are connected to the central Mn_4 unit by eight bridging μ_3-O^{2-} ions. The metal oxidation states and their trapped-valence nature were determined by inspection of the Mn$-$O

Table 1. Crystallographic Data for Complexes **1a**, **1b**, **2**, **4**, **5**

param	**1a**	**1b**	**2**	**4**	**5**
formula	$C_{150}H_{174}Cl_8Mn_{12}N_2O_{50}{}^a$	$C_{147}H_{168}Cl_2Mn_{12}N_2O_{50}{}^b$	$C_{15}H_{13}MnO_5$	$C_{62}H_{64}Mn_4O_{24}{}^c$	$C_{134}H_{134}Cl_{12}Mn_{12}NO_{47}{}^d$
fw	3747.90	3493.09	328.19	1412.89	3595.10
space group	Pbca	$P\bar{1}$	$P\bar{1}$	$P\bar{1}$	$P2_1/c$
a, Å	25.476(2)	16.357(1)	6.776(1)	11.144(1)	20.412(2)
b, Å	20.933(2)	17.480(2)	10.074(2)	11.819(1)	21.452(2)
c, Å	31.206(2)	17.617(2)	11.314(2)	12.465(1)	35.657(2)
β, deg	90	111.329(2)	79.478(2)	94.589(2)	94.933(2)
V, Å³	16 642(2)	3982.5(4)	757.6(2)	1585.1(2)	15 555(2)
Z	4	1	2	1	4
T, K	173	173	173	173	173
radiatn	Mo Kα	Mo Kα	Mo Kα	Mo Kα	Mo Kα
ρ_{calcd}, g/cm³	1.502	1.348	1.439	1.480	1.535
μ, mm⁻¹	1.086	1.024	0.888	0.859	1.223
R1^{e,f}	6.42	6.96	5.45	4.88	5.54
wR2^{e,g}	15.85	17.31	10.85	10.98	10.44

^{a} Including two water and four dichloromethane solvate molecule. ^{b} Including two water and one dichloromethane solvate molecules. ^{c} Including two methanol solvate molecules. ^{d} Including six dichloromethane solvate molecules. ^{e} $I > 2\sigma(I)$. ^{f} R1 $= 100\Sigma(||F_o| - |F_c||)/\Sigma|F_o|$. ^{g} wR2 $= 100[\Sigma[w(F_o{}^2 - F_c{}^2)^2]/\Sigma[w(F_o{}^2)^2]]^{1/2}$; $w = 1/[\sigma^2(F_o{}^2) + [(ap)^2 + bp]$, where $p = [\max(F_o{}^2, 0) + 2F_c{}^2]/3$.
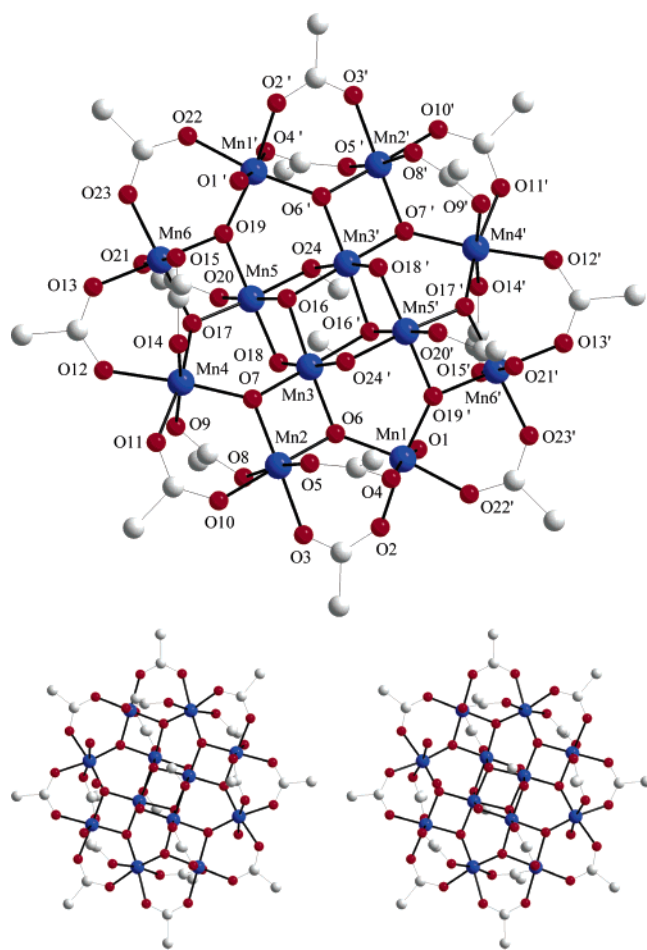
Figure 1. Labeled PovRay representation and stereopair at the 50% probability level of the anion of **1a**. For clarity, the benzoate rings have been omitted, except for the *ipso*-carbon atom of each ring. Color scheme: Mn (blue); O (red); C (gray).

bond lengths, Mn bond valence sum calculations,[22] and the presence of Mn^III Jahn−Teller elongation axes on the Mn atoms in the outer ring. The central [Mn^IV₄O₄(OMe)₂]^6+ unit comprises a planar Mn₄ rhombus with two μ_3-O²⁻ ions (O16,

(22) (a) Bond valence sum calculations for Mn^III and Mn^IV ions of **2a,b** gave oxidation state values of 2.89−3.02 and 4.00−4.18, respectively. (b) Liu, W.; Thorp, H. H. *Inorg. Chem.* **1993**, *32*, 4102.

Table 2. Selected Interatomic Distances (Å) for **1·2H₂O·4CH₂Cl₂**

Mn1−O19′	1.878(4)	Mn4−O17	1.891(4)
Mn1−O6	1.905(4)	Mn4−O7	1.958(4)
Mn1−O22′	1.981(4)	Mn4−O11	1.988(4)
Mn1−O2	1.990(4)	Mn4−O12	2.060(5)
Mn1−O4	2.112(5)	Mn4−O9	2.074(4)
Mn1−O1	2.226(4)	Mn4−O14	2.080(5)
Mn2−O7	1.883(4)	Mn5−O18	1.842(4)
Mn2−O6	1.897(4)	Mn5−O16	1.875(4)
Mn2−O3	1.950(4)	Mn5−O17	1.876(4)
Mn2−O10	1.976(4)	Mn5−O24	1.904(4)
Mn2−O5	2.177(4)	Mn5−O19	1.918(4)
Mn2−O8	2.233(4)	Mn5−O20	1.932(4)
Mn3−O18	1.857(4)	Mn6−O19	1.876(4)
Mn3−O7	1.881(4)	Mn6−O17	1.877(4)
Mn3−O6	1.892(4)	Mn6−O23	1.930(4)
Mn3−O16	1.901(4)	Mn6−O13	1.947(4)
Mn3−O16′	1.934(4)	Mn6−O15	2.214(5)
Mn3−O24′	1.939(4)	Mn6−O21	2.250(5)

Table 3. Selected Interatomic Distances (Å) for **1·2H₂O·CH₂Cl₂**

|			
Mn1−O18′	1.935(3)	Mn4−O16	1.895(3)
Mn1−O3	1.948(3)	Mn4−O11	1.917(3)
Mn1−O23′	1.997(4)	Mn4−O15	1.956(4)
Mn1−O2	2.009(4)	Mn4−O13	1.970(4)
Mn1−O1	2.026(4)	Mn4−O14	2.111(4)
Mn1−O25′	2.105(5)	Mn4−O12	2.157(4)
Mn2−O11	1.897(3)	Mn5−O16	1.860(3)
Mn2−O3	1.900(3)	Mn5−O18	1.869(3)
Mn2−O5	1.942(4)	Mn5−O9	1.873(3)
Mn2−O6	1.948(5)	Mn5−O10	1.886(3)
Mn2−O7	2.161(5)	Mn5−O17	1.906(3)
Mn2−O4	2.173(5)	Mn5−O8′	1.909(3)
Mn3−O3	1.873(3)	Mn6−O16	1.891(3)
Mn3−O11	1.875(3)	Mn6−O22	1.953(3)
Mn3−O10	1.882(3)	Mn6−O21	1.961(4)
Mn3−O9	1.919(2)	Mn6−O19	2.208(4)
Mn3−O8	1.921(3)	Mn6−O20	2.233(4)
Mn3−O9′	1.930(3)	Mn6−O18	1.879(3)

O16′), one above and one below the Mn₄ plane, and a μ-O²⁻ (O18, O18′) or μ-MeO⁻ (O24, O24′) ion bridging each edge. The central unit can thus be described either as a face-sharing dicubane unit with two vertexes missing or as two edge-sharing, oxide-capped Mn₃ triangular units. Tetranuclear complexes possessing such a core, or one very similar, have been observed previously with Mn,[5a,b] as well as with other transition metals.[23] Peripheral ligation is completed by 16 bridging benzoate groups and 2 terminal water molecules. The outer Mn₈ ring of [Mn₁₂′]²⁻ is very similar to that in

normal Mn_{12} compounds, but the latter contain a central $[Mn_4(\mu_3\text{-O})_4]^{8+}$ cubane; i.e., the central Mn_4 topology is a tetrahedron and not a rhombus.

Complex **1b** crystallizes in the triclinic space group $P\bar{1}$, with the $[Mn_{12}']^{2-}$ anion again lying on a crystallographic center of symmetry. The structure of the $[Mn_{12}']^{2-}$ anion of **1b** is essentially identical with that of **1a**, except for some disorder in the peripheral benzoate rings and is thus not discussed further here; full details are available in the Supporting Information.

For both **1a,b**, there are Jahn−Teller (JT) distortions at the Mn^{III} ions in the outer ring, consistent with high-spin Mn^{III} in near-octahedral geometry. The JT distortion takes the form of an axial elongation, as is the usual case for octahedral Mn^{III}, with the elongation axes axial to the Mn_{12} disklike core and thus roughly parallel to each other. Axially elongated Mn−O bonds are typically at least 0.1−0.2 Å longer than the others. However, there is one anomaly: for **1a** (Figure 1), the JT elongated bonds at Mn4 (Mn4−O9 = 2.074(4), Mn4−O14 = 2.080(5) Å) are not as long as those at the other Mn^{III} ions (2.112(5)−2.250(5) Å), and trans bonds Mn4−O7 (1.958(4)Å) and Mn4−O12 (2.060(5)Å) are longer than expected, especially Mn−O7, which is unusually long for a Mn−O^{2-} bond (compare Mn−O^{2-} bonds at the other Mn^{III} ions of 1.876(4)−1.905(4)Å). A similar anomalous situation is present at Mn1 of **1b**. This structural feature at Mn atoms Mn4 of **1a** and Mn1 of **1b** suggest a static disorder of JT elongation axes about two orientations, and indeed this will prove crucial to our understanding and interpretation of the magnetic data to be discussed below. We will return to this point later, at which point the anomalous bond lengths will be discussed in greater detail.

As mentioned above, the $[Mn_{12}']^{2-}$ anions of **1a,b** are overall very similar to normal Mn_{12} clusters, such as **1**, with the main difference being the structure of the central core units. These are compared in Figure 2. In fact, the core of the anions of **1a,b** could be considered the result of partial methanolysis of the central $[Mn_4O_4]^{8+}$ cubane of a normal Mn_{12}, leading to incorporation of two MeO^- bridges and a change in the core structure. However, we are merely pointing out a structural relationship and do not claim that methanolysis of normal Mn_{12} represents the pathway of the formation of **1** in the reaction solution. On the contrary, for reasons outlined earlier, we suspect that the $[Mn_{12}']^{2-}$ complexes are the precursors to the normal Mn_{12} (eq 5) and not the other way around. It is also interesting to note that the $[Mn_{12}']^{2-}$ anion of **1** and the normal Mn_{12} complexes are the smallest nuclearity members of a larger family of $[Mn^{III}_x, Mn^{IV}_y]$ clusters in which there is an outer Mn^{III}_x ring around a central Mn^{IV}_y core. This family currently comprises normal Mn_{12} complexes (such as **3**) and **1a**/**1b** ($x = 8$, $y = 4$), the Mn_{16} cluster $[Mn_{16}O_{16}(OMe)_6(O_2CMe)_{16}(MeOH)_3\text{-}$
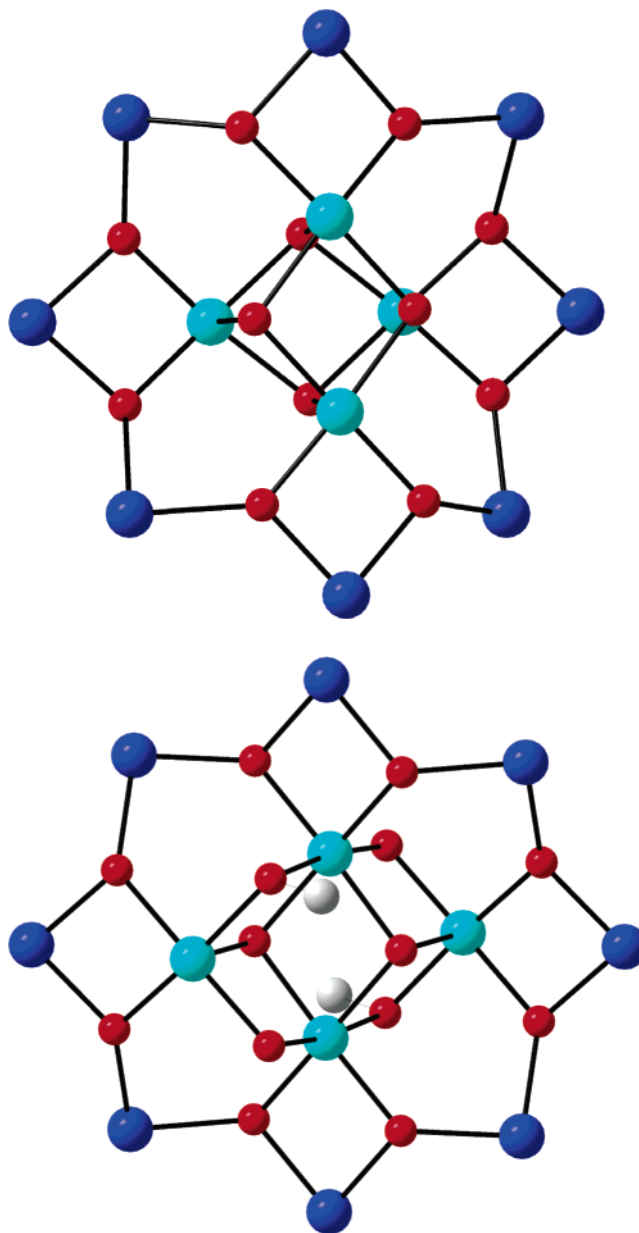
Figure 2. Comparison of the cores of the anion of **1a** (bottom) and normal Mn_{12} complex **3** (top). Color scheme: Mn^{4+} (cyan); Mn^{3+} (blue); O (red); C (gray).

$(H_2O)_3]$ ($x = 10$, $y = 6$),[4c,11] and the Mn_{21} cluster $[Mn_{21}O_{24}(OMe)_8(O_2CCH_2{}^tBu)_{16}(H_2O)_{10}]$ ($x = 12$, $y = 9$).[24]

A PovRay representation of a small section of the polymeric chain of compound **2** is shown in Figure 3, and selected interatomic distances are listed in Table 4. Compound **2** crystallizes in the triclinic space group $P\bar{1}$ with the asymmetric unit consisting of the $[Mn^{III}_{1/2}(\mu\text{-OMe})(\mu\text{-}O_2CPh)_2Mn^{III}_{1/2}]$ repeating unit of a $[Mn^{III}(OMe)(O_2CPh)_2]_n$ linear chain (Figure 3). The structure of **2** is overall similar to that of $\{[Mn(OH)(O_2CMe)_2]\cdot HO_2CMe\cdot H_2O\}_n$ (**7**) reported recently,[25] which is also a linear chain, except that (i) there

(23) For example, see: (a) Manos, M. J.; Tasiopoulos, A. J.; Tolis, E. J.; Lalioti, N.; Woolins, J. D.; Slawin, A. M. Z.; Sigalas, M. P.; Kabanos, T. A. *Chem.—Eur. J.* **2003**, *9*, 695. (b) Kang, H.; Liu, S.; Shaikh, S. N.; Nicholson, T.; Zubieta, J. *Inorg. Chem.* **1989**, *28*, 920.

(24) Brockman, J. T.; Huffman, J. C.; Christou, G. *Angew. Chem., Int. Ed.* **2002**, *41*, 2506.

(25) (a) Tasiopoulos, A. J.; Harden, N. C.; Abboud, K. A.; Christou, G. *Polyhedron* **2003**, *22*, 133. (b) Price, D. J.; Batten, S. R. Moubaraki, B.; Murray, K. S. *Polyhedron* **2003**, *22*, 2167.
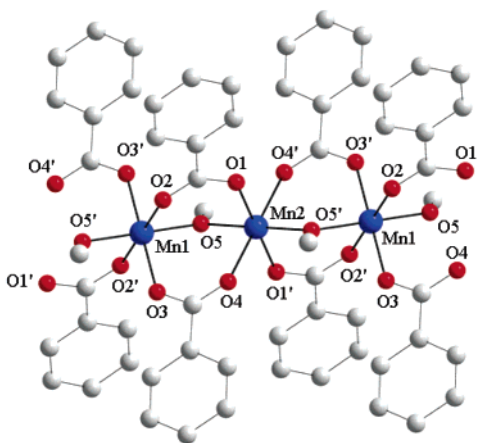
Figure 3. Labeled PovRay representation (at the 50% probability level) of a small section of the polymeric chain of $[Mn(OMe)(O_2CPh)_2]_n$ (**2**).

Table 4. Selected Interatomic Distances (Å) for **2**

Mn1−O5′	1.928(3)	Mn2−O5	1.931(2)
Mn1−O5	1.928(3)	Mn2−O5′	1.931(2)
Mn1−O3′	1.928(3)	Mn2−O1	1.932(3)
Mn1−O3	1.928(3)	Mn2−O1′	1.932(3)
Mn1−O2	2.162(3)	Mn2−O4	2.152(3)
Mn1−O2′	2.162(3)	Mn2−O4′	2.152(3)

are OMe⁻ bridging groups instead of OH⁻, (ii) the carboxylate ligands are PhCO₂⁻ instead of MeCO₂⁻, and (iii) there are no solvent molecules of crystallization. Point iii is in contrast to complex **7**, where H₂O and MeCO₂H molecules form a hydrogen-bonding network linking the chains. The Mn···Mn separations in **2** are 3.388(1) Å, identical with the 3.384(1) Å value of those in **7**, and all of the PhCO₂⁻ groups are in their familiar *syn,syn*-bridging modes. The metal oxidation states of the two independent Mn atoms were determined by inspection of the Mn−O bond lengths, Mn bond valence sum calculations,[22b,26] and the presence of Mn^III Jahn−Teller elongation axes, as expected for high-spin Mn^III in near-octahedral geometry. The Jahn−Teller elongation axes are O(2)−Mn(1)−O(2′) and O(4′)−Mn−O(2), which are near-parallel. It is interesting to note that the [Mn(μ-OMe)(μ-O₂CR)₂Mn] triply bridged unit is unprecedented in any Mn cluster of any nuclearity; in fact, there are relatively few Mn complexes of any type containing bridging methoxide groups. A close examination of the packing of **2** shows that the chains all run parallel in the crystal, and in the absence of solvent molecules of crystallization there are no hydrogen-bonding interactions linking neighboring chains. However, closer inspection reveals π-stacking interactions between the benzoate phenyl rings of neighboring chains (average C···C separation = 3.719 Å). This is emphasized in Figure 4, which shows a small part of two adjacent chains from a viewpoint perpendicular to the chains.

A PovRay representation of complex **4** is shown in Figure 5, and selected interatomic distances are listed in Table 5. Complex **4**·2MeOH crystallizes in the triclinic space group P1̄ and contains a [Mn₄O₂(O₂CPh)₈(MeOH)₄] cluster lying on an inversion center. The cluster possesses an [Mn₄O₂]⁸⁺

(26) Bond valence sum calculations for the two independent Mn^III ions of **2** gave oxidation state values of 2.98 for both of them.
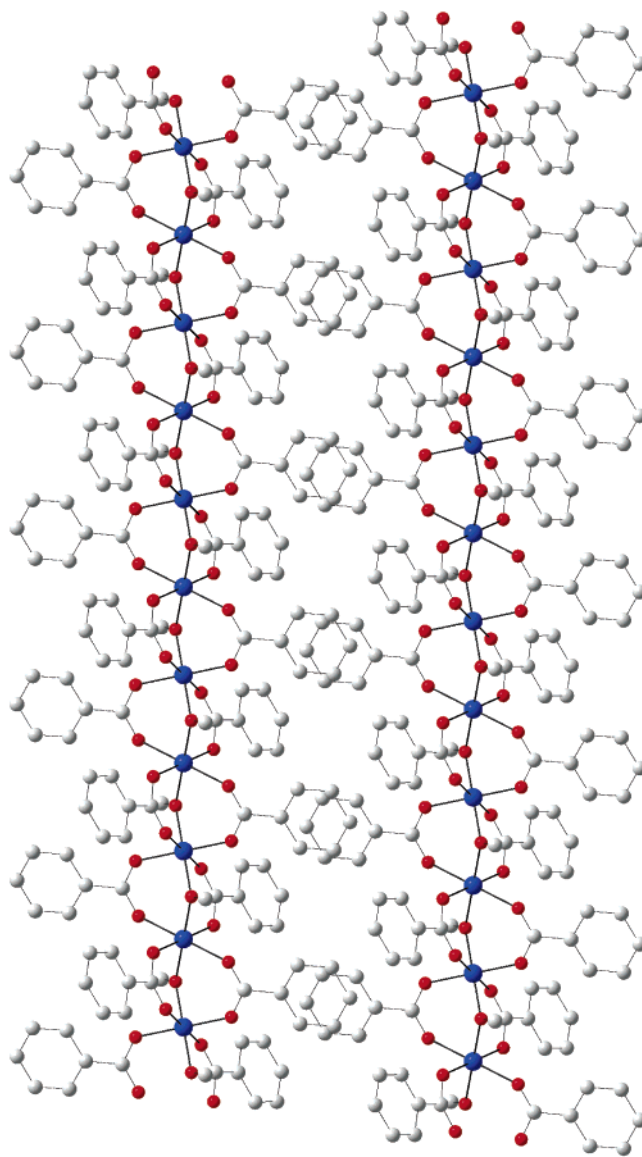
Figure 4. Section of two adjacent chains of **2** emphasizing the π-stacking between benzoate rings of neighboring chains.
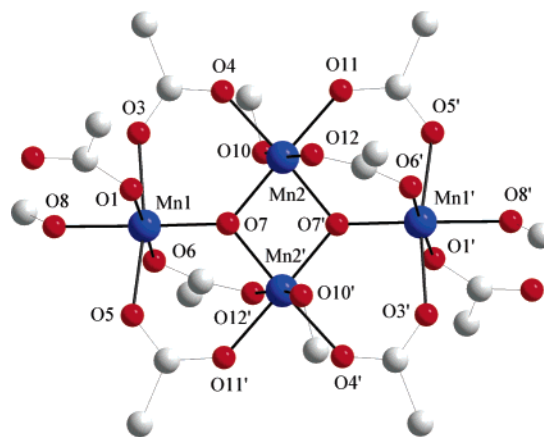
Figure 5. Labeled PovRay representation (at the 50% probability level) of **4**. For clarity, the benzoate rings have been omitted, except for the *ipso*-carbon atom of each ring. Color scheme: Mn (blue); O (red); C (gray).

(4Mn^III) core[22b,27] with a planar Mn₄ rhombus and a μ_3-O²⁻ ion above and below this plane. The core is thus of the type that we have described as "planar butterfly" in the past, to

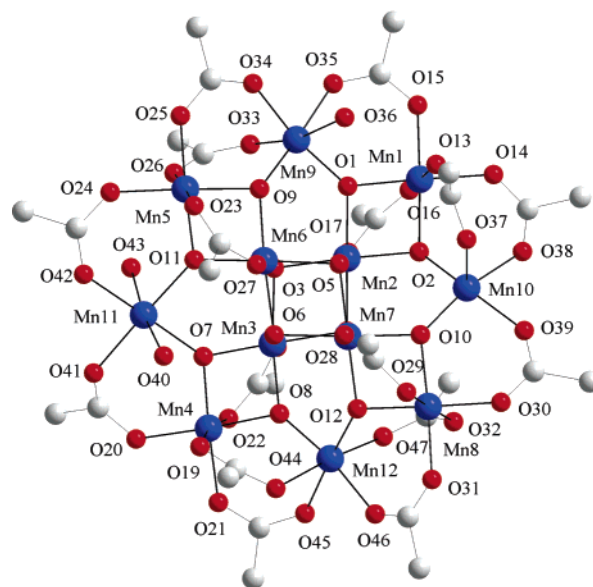**Table 5.** Selected Interatomic Distances (Å) for **4**·2MeOH

Mn1−O7	1.843(2)	Mn2−O7	1.903(2)
Mn1−O6	1.950(2)	Mn2−O4	1.945(2)
Mn1−O8	1.973(2)	Mn2−O11	1.947(2)
Mn1−O1	1.998(2)	Mn2−O12	2.156(2)
Mn1−O5	2.138(2)	Mn2−O10	2.271(2)
Mn1−O3	2.144(2)	Mn2····Mn2′	2.8929(7)
Mn2−O7′	1.892(2)		

emphasize its relationship to the related $[Mn_4O_2]^{8+}$ complexes with a true butterfly topology (i.e. V-shaped Mn_4). In fact, complex **4** is overall very similar to the $[Mn_4O_2(O_2CPh)_9-(H_2O)]^-$ (**8**) anion, even though the latter has a true butterfly core,[28] in that they both contain only carboxylate and H_2O/MeOH peripheral ligands. The structural difference is primarily the consequence of **8** having a bridging carboxylate group between the two central ("body") Mn atoms, which has always been found to cause a bending of the Mn_4 topology to V-shaped, whereas **4** has a terminal MeOH group on each of these two Mn atoms (Mn2 and Mn2′) and is thus planar. In addition, **4** has a terminal MeOH and a monodentate carboxylate on each "wingtip" Mn atom (Mn1 and Mn1′), whereas **8** has a terminal carboxylate and H_2O at one wingtip Mn atom but a chelating carboxylate at the other.

Examination of the unit cell of **4**·2MeOH reveals both intra- and intermolecular hydrogen-bonding: the unbound O atom of the monodentate benzoate group on Mn1 is hydrogen-bonded to the adjacent bound MeOH group ($O(2)$···$O(8) = 2.551(2)$ Å), whereas the bound O of this same carboxylate group is hydrogen-bonded to a lattice MeOH ($O1$···$O9 = 2.799(2)$ Å), which also hydrogen bonds to the bound MeOH group on Mn2 of a neighboring molecule ($O9$···$O10 = 2.677(2)$ Å).

A PovRay representation of complex **5**·6CH_2Cl_2 is shown in Figure 6, and selected interatomic distances are listed in Table 6. Complex **5**·6CH_2Cl_2 crystallizes in the monoclinic space group $P2_1/c$ with the $[Mn_{12}]^-$ anion in a general position. The $[Mn_{12}O_{12}(O_2CPh)_{16}(H_2O)_3]^-$ anion is similar in many aspects to the previously characterized[6f,9] $[Mn_{12}O_{12}-(O_2CR)_{16}(H_2O)_4]^-$ complexes and especially with the $[Mn_{12}O_{12}(O_2CPh)_{16}(H_2O)_4]^{-9a}$ anion, which also contains benzoate groups. Nevertheless, there is an interesting difference with the latter in that the anion of **5** contains only three bound H_2O molecules, and one Mn^{III} ion (Mn10) is thus five-coordinated. Charge considerations, inspection of metric parameters, bond valence sum calculations,[22b,29] and the presence of Mn^{III} Jahn−Teller elongation axes establish a trapped-valence $Mn^{IV}_4Mn^{III}_7Mn^{II}$ situation in the anion of **5**, with Mn11 being the Mn^{II} ion.

Electrochemistry. As described above, **1** is structurally similar to the normal Mn_{12} family of complexes that exhibit

(27) Bond valence sum calculations for the two independent Mn^{III} ions of **4** gave oxidation state values of 2.95−2.97.
(28) (a) Wemple, M. W.; Tsai, H.-L.; Wang, S.; Claude, J. P.; Streib, W. E.; Huffman, J. C. Hendrickson, D. N.; Christou, G. *Inorg. Chem.* **1996**, *35*, 6437. (b) Wang, S.; Huffman, J. C.; Folting, K.; Streib, W. E.; Lobkovsky, E. B.; Christou, G. *Angew. Chem., Int. Ed. Engl.* **1991**, *30*, 1672.
(29) Bond valence sum calculations gave oxidation state values 1.99, 2.93−3.03, and 3.97−4.18 for the one Mn^{II}, seven Mn^{III}, and four Mn^{IV} ions of **5**, respectively.

Figure 6. Labeled PovRay representation (at the 50% probability level) of **5**·6CH_2Cl_2. For clarity, the benzoate rings have been omitted, except for the *ipso*-carbon atom of each ring. Color scheme: Mn (blue); O (red); C (gray).

Table 6. Selected Interatomic Distances (Å) for **5**·6CH_2Cl_2

Mn1−O1	1.885(2)	Mn7−O10	1.881(2)
Mn1−O2	1.894(3)	Mn7−O4	1.889(2)
Mn1−O15	1.941(3)	Mn7−O5	1.898(3)
Mn1−O14	1.947(3)	Mn7−O12	1.902(3)
Mn1−O16	2.169(3)	Mn7−O6	1.914(2)
Mn1−O13	2.197(3)	Mn7−O28	1.934(3)
Mn2−O1	1.880(3)	Mn8−O12	1.890(2)
Mn2−O2	1.890(2)	Mn8−O10	1.911(3)
Mn2−O4	1.893(3)	Mn8−O30	1.957(3)
Mn2−O5	1.893(2)	Mn8−O31	1.960(3)
Mn2−O3	1.896(2)	Mn8−O32	2.095(3)
Mn2−O17	1.933(3)	Mn8−O29	2.184(3)
Mn3−O7	1.824(2)	Mn9−O1	1.882(2)
Mn3−O8	1.842(3)	Mn9−O9	1.890(2)
Mn3−O6	1.907(2)	Mn9−O34	1.958(3)
Mn3−O18	1.925(2)	Mn9−O35	1.968(3)
Mn3−O3	1.957(3)	Mn9−O33	2.112(3)
Mn3−O4	1.961(2)	Mn9−O36	2.271(3)
Mn4−O7	1.874(3)	Mn10−O10	1.862(3)
Mn4−O8	1.891(2)	Mn10−O2	1.867(2)
Mn4−O20	1.951(3)	Mn10−O39	1.929(3)
Mn4−O21	1.977(3)	Mn10−O38	1.944(3)
Mn4−O22	2.194(3)	Mn10−O37	2.093(3)
Mn4−O19	2.241(3)	Mn11−O11	2.066(3)
Mn5−O11	1.865(3)	Mn11−O41	2.099(3)
Mn5−O9	1.924(2)	Mn11−O42	2.115(3)
Mn5−O25	1.956(3)	Mn11−O7	2.129(2)
Mn5−O24	1.958(3)	Mn11−O43	2.224(4)
Mn5−O26	2.157(3)	Mn11−O40	2.249(3)
Mn5−O23	2.280(3)	Mn12−O8	1.869(3)
Mn6−O11	1.818(2)	Mn12−O12	1.904(3)
Mn6−O9	1.875(3)	Mn12−O46	1.977(3)
Mn6−O3	1.910(2)	Mn12−O45	1.977(3)
Mn6−O27	1.934(3)	Mn12−O47	2.149(3)
Mn6−O6	1.943(3)	Mn12−O44	2.161(3)
Mn6−O5	1.947(2)		

multiple reversible redox processes. In fact, knowledge of the latter allowed isolation of the one- and two-electron-reduced forms, $[Mn_{12}]^-$ and $[Mn_{12}]^{2-}$. The redox properties of **1** were thus investigated by cyclic voltammetry (CV) in CH_2Cl_2 solution. The CV of **1** is somewhat similar to that of normal Mn_{12} in exhibiting three redox processes, one oxidation and two reductions, but these are now irreversible.
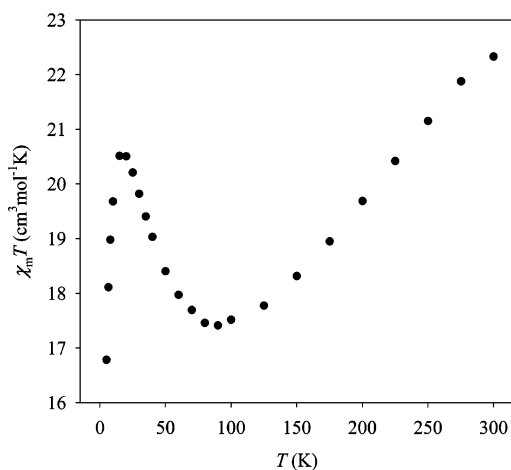
Figure 7. Plot of $\chi_m T$ vs T for dried complex **1**·2H₂O.

Figure 8. Plot of $\chi_m T$ vs T for **2**.

The two reductions were at $E_{1/2} = -0.402$ and 0.083 V with peak separations (at a scan rate 100 mV/s) of 730 and 500 mV, respectively. The oxidation process was at $E_{1/2} = 0.578$ V with a peak separation of 510 mV. The ratio i_f/i_r of the forward and reverse currents for the three processes was in the range 0.80−1.00. Thus, the structural differences between **1** and normal Mn₁₂ did not preclude observation of the same oxidation and reduction processes but did drastically affect their reversibility.

Direct Current Magnetic Susceptibility Studies. Solid-state, variable-temperature magnetic susceptibility measurements were performed on vacuum-dried microcrystalline samples of **1**·2H₂O, **2**, and **5**·H₂O, all suspended in eicosane to prevent torquing. The dc magnetic susceptibility (χ_m) data were collected in the 5.0−300 K range in a 0.5 T (T) magnetic field. The experimental data for **1**·2H₂O are plotted as $\chi_m T$ vs T in Figure 7. The $\chi_m T$ value decreases from 22.33 cm³ mol⁻¹ K at 300 K to a minimum of 17.41 cm³ mol⁻¹ K at 90 K and then increases to 20.51 cm³ mol⁻¹ K at 15 K before again decreasing to 16.78 at 5.0 K. The spin-only ($g = 2$) $\chi_m T$ value for a cluster containing 8Mn^III and 4Mn^IV noninteracting ions is 31.5 cm³ mol⁻¹ K, so the observed value at 300 K suggests the existence of strong antiferromagnetic interactions. If we assume the drop at <15 K is due to Zeeman and anisotropy effects, then the $\chi_m T$ peak value of 20.51 cm³ mol⁻¹ K at 15 K is consistent with an $S = 6$ ground state, for which the spin-only ($g = 2$) value is 21.00 cm³ mol⁻¹ K.

The data for complex **2** are plotted as $\chi_m T$ vs T in Figure 8. The $\chi_m T$ value of 2.59 cm³ mol⁻¹ K at 300 K is significantly lower than the expected spin-only ($g = 2$) value of 3.0 cm³ mol⁻¹ K for an isolated Mn^III center; it then decreases steadily to 0.18 cm³ mol⁻¹ K at 8.0 K and then increases smoothly to 0.21 at 5.0 K. These data suggest the existence of strong antiferromagnetic interactions between the Mn^III centers of the chain, resulting in a diamagnetic ground state ($S = 0$). This is not surprising because triply bridged Mn₂^III (and Mn^IIMn^III) dinuclear units are almost always antiferromagnetically coupled, although a dinuclear complex with the [Mn(μ-OMe)(μ-O₂CR)₂Mn] core is not known for direct comparison. The very small increase at $T < 8$ K could be due to weak ferromagnetism from spin
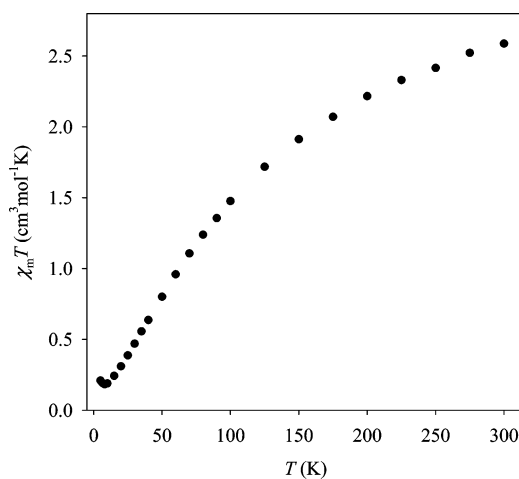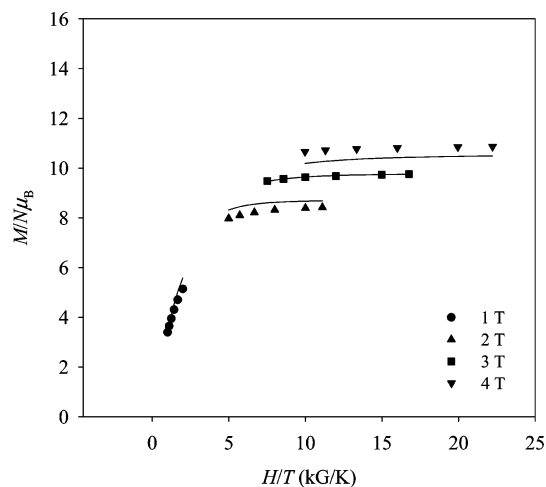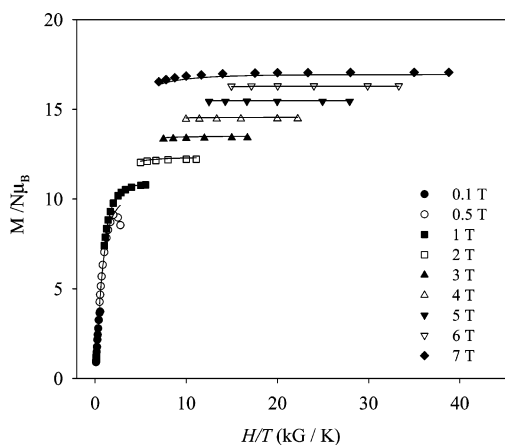

Figure 9. Plot of $M/N\mu_B$ vs H/T for dried complex **1**·2H₂O at the indicated applied fields. The solid lines are fits of the data; see the text for the fit parameters.

canting within the chains. This behavior is similar to that observed for complex **7**, where however this behavior is more pronounced, presumably due to the stronger interactions between chains mediated by the strong hydrogen-bonding in **7**.[25] For **5**·H₂O, the $\chi_m T$ value of 21.14 cm³ mol⁻¹ K at 300 K decreases steadily to a value of 18.68 cm³ mol⁻¹ K at 175 K and then increases to 50.56 at 15 K before decreasing to 41.04 cm³ mol⁻¹ K at 5.0 K. This behavior is very similar to those observed for other, previously studied salts of the [Mn₁₂O₁₂(O₂CR)₁₆(H₂O)ₓ]⁻ ($x = 3$ or 4)[6f,9] anion.

To characterize the ground states of complexes **1**·2H₂O and **5**·H₂O, magnetization (M) data were collected in the 0.1−7.0 T field range and 1.80−10.00 K temperature range. Shown in Figures 9 and 10 are the obtained data for **1**·2H₂O and **5**·H₂O, respectively, plotted as reduced magnetization ($M/N\mu_B$) versus H/T, where N is Avogadro's number and μ_B is the Bohr magneton. For a system occupying only the ground state and experiencing no zero-field splitting (ZFS), the various isofield lines would be superimposed and $M/N\mu_B$ would saturate at a value of gS. The nonsuperimposition of the isofield lines clearly indicates the presence of ZFS. The data were fit using the program MAGNET,[17] which assumes that only the ground state is populated at these temperatures,

Figure 10. Plot of $M/N\mu_B$ vs H/T for dried complex **5·H$_2$O** at the indicated applied fields. The solid lines are fits of the data; see the text for the fit parameters.
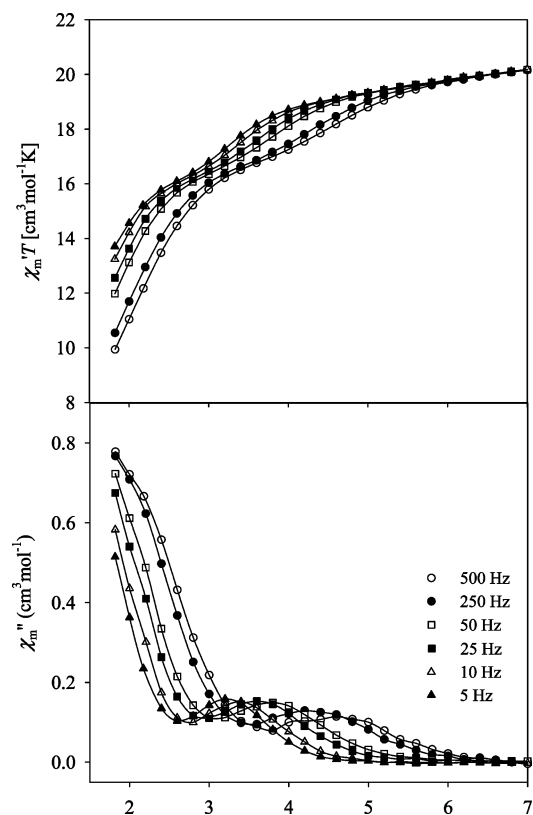

Figure 11. Out-of-phase (χ_m'') ac susceptibility signals for a wet microcrystalline sample of complex **1** at the indicated frequencies.

includes axial ZFS and the Zeeman interaction with the applied field, and carries out a full powder average. For complex **1·2H$_2$O**, it was not possible to obtain a good fit when all the data collected at all fields were used. In our experience, the usual reason for this is the population of one or more excited states, either because (i) these excited states are close enough to the ground state that they have a nonzero Boltzmann population even at the low temperatures used in the magnetization study or (ii) even excited states that are more separated from the ground state but have an S value greater than that of the ground-state become populated as their larger M_S levels rapidly decrease in energy due to the applied magnetic field and approach (or even cross) those of the ground state. Either (or both) of these two effects will lead to poor fits, since the fitting program assumes population of only the ground state. As we have described elsewhere on multiple occasions,[4f–h] one way around effect ii is to use only data collected at low fields. Indeed, a reasonable fit of the reduced magnetization data could be achieved when data collected in fields only up to 4 T were employed, suggesting that effect ii is the main cause of the fitting problems. (As shown below, dried **1·2H$_2$O** contains two species, which no doubt also affects the quality of the magnetization fit.) The fit is shown as the solid line in Figure 9, and the fit parameters were $S = 6$, $g = 1.96(2)$, and $D = -0.37(2)$ cm^{-1}. This fit is also consistent with the $\chi_m T$ data in Figure 7, whose values in the 5–15 K range of ~17–20.5 cm^3 mol^{-1} K are consistent with an $S = 6$ ground state (spin-only ($g = 2$) value of 21.0 cm^3 mol^{-1} K, as stated earlier) and $g < 2$, as expected for Mn. The spin-only values for $S = 5$ and $S = 7$ are 15 and 28 cm^3 mol^{-1} K, respectively; the appropriate relationship is $\chi_m T = (g^2/8)S(S + 1)$, or $\chi_m T = S(S + 1)/2$ for $g = 2$.

In contrast to the fitting problems encountered for complex **1·2H$_2$O**, the reduced magnetization data for complex **5·H$_2$O** collected at all fields up to 7 T were fit very well, with fit parameters of $S = 19/2$, $g = 2.00(1)$, and $D = -0.40(1)$ cm^{-1}. This fit is shown as the solid line in Figure 10. The $S = 19/2$ ground state is in agreement with that observed for several previous examples of one-electron-reduced normal Mn$_{12}$ complexes.[6f,9a]
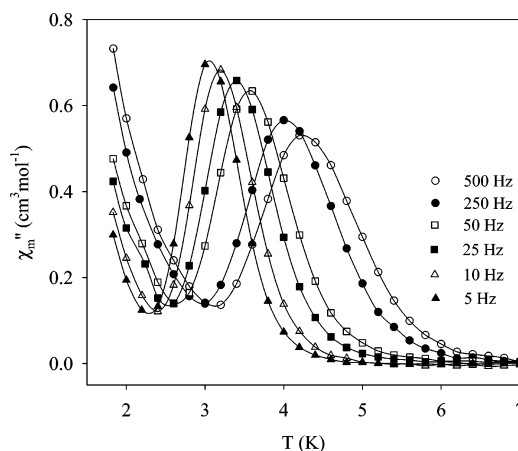
Alternating Current Magnetic Susceptibility Studies. In an ac susceptibility experiment, a weak field (typically 1–5 G) oscillating at a particular frequency (ν) is applied to a sample to probe the dynamics of the magnetization (magnetic moment) relaxation. Alternating current susceptibility studies were performed on both vacuum-dried and wet (with mother liquor) polycrystalline samples of **1** (containing both **1a,b**) and **5** in the temperature range 1.8–10 K in a zero dc field and a 3.5 G ac field oscillating at frequencies in the 5–1500 Hz range.

The structural similarity between complexes **1** and **3** as well as the high S and D values that were determined from reduced magnetization measurements of **1** suggested the possibility that it might also be a SMM, just like **3**. Indeed, ac magnetic susceptibility studies on a wet sample of **1** suspended in eicosane revealed two frequency-dependent out-of-phase (χ_m'') ac signals (Figure 11), one in the higher temperature (HT) range of 3–5 K and a second one at lower temperatures (LT) whose peaks clearly occur at temperatures below the operating limit of our SQUID instrument (1.8 K). The LT and HT χ_m'' signals correspond to faster and slower relaxation rates, respectively. When the ac magnetic susceptibility studies were instead carried out on a vacuum-dried microcrystalline sample of **1·2H$_2$O** suspended in eicosane (Figure 12), two χ_m'' signals were again observed and at the same temperature ranges as those of the wet sample. However, the HT signal was now very weak whereas the LT signal was significantly stronger, suggesting that removal of the solvent of crystallization causes a conversion of the HT form to the LT form. We have seen on several occasions that very different results are obtained on wet crystals vs vacuum-dried solid, and the results obtained on complex **1** emphasize this point again.

We have noted elsewhere on multiple occasions that the in-phase ac susceptibility signal (χ_m') is a useful way to determine the ground-state spin S of a molecule, particularly when there are complications from low-lying excited states that interfere with determination of S from dc magnetization fits.[4f,g,11] In the absence of slow magnetization relaxation, i.e., in the absence of an out-of-phase (χ_m'') signal, the in-phase ac susceptibility should be equivalent to the dc
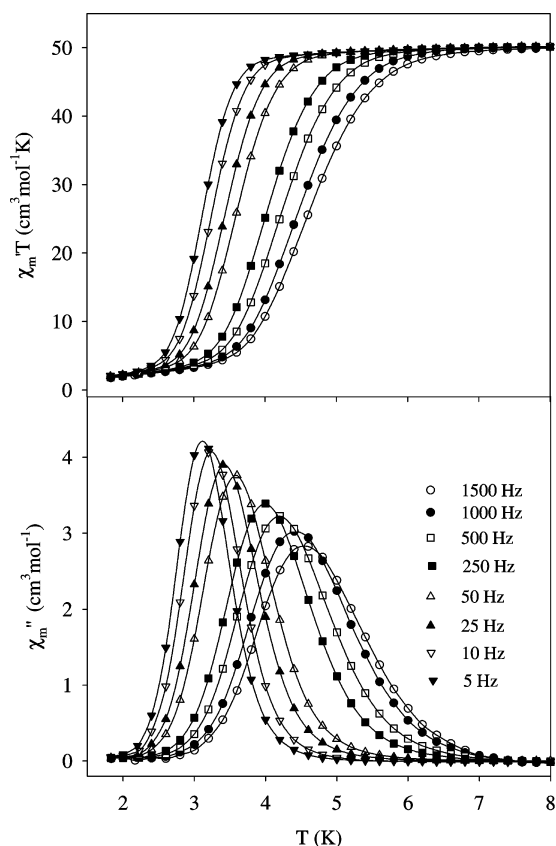
Figure 12. In-phase (χ_m') and out-of-phase (χ_m'') ac susceptibility signals for a vacuum-dried microcrystalline sample of complex **1·2H₂O** at the indicated frequencies.


Figure 13. In-phase (χ_m') and out-of-phase (χ_m'') ac susceptibility signals for a vacuum-dried microcrystalline sample of complex **5·H₂O** at the indicated frequencies.

susceptibility. This route to the susceptibility thus avoids the potential complications of measurements in an applied dc field, since the ac experiment uses only a very weak ac field. Extrapolation of the in-phase $\chi_m'T$ signal of dried **1·2H₂O** in Figure 12 from >6 K down to 0 K, avoiding the drops due to the onset of slow magnetization relaxation, gives a value of ~18 cm³ mol⁻¹ K, which corresponds to an $S = 6$ ground state with $g = 1.85$, in satisfying agreement with the results of the dc magnetization fits above. In contrast, $S = 5$ and 7 ground states would be expected to give values of slightly less than 15 and 28 cm³ mol⁻¹ K, respectively.

It is tempting to assume that the two χ_m'' signals in Figure 11 for wet samples of **1** are due to the two crystal forms that are present, diamond-like **1a** and needlelike **1b**. However, this would represent rather a large difference for species differing only in the solvent molecules of crystallization. Additional studies were required to address this point further, and these were provided by the hysteresis determinations discussed later.

In contrast to the above, the in-phase and out-of-phase ac magnetic susceptibility signals of the vacuum-dried and wet samples of **5** are identical; the data for the dried solid (**5·H₂O**) are shown in Figure 13. The out-of-phase (χ_m'') plot shows a single, frequency-dependent signal in the 3−5 K range. Extrapolation of the $\chi_m'T$ plot from its plateau in the 6−8 K range to 0 K gives a value of ~49 cm³ mol⁻¹ K, which corresponds to an $S = 19/2$ ground state with $g \sim 2$, confirming the results of the dc magnetization fits described above.

The peak of a χ_m'' vs T plot represents the temperature at which the magnetization relaxation rate equals the angular frequency ω ($=2\pi\nu$), and the χ_m'' vs T data at different frequencies (ν) for wet samples of complexes **1** and **5** were therefore used as a source of rate vs T kinetic data to construct Arrhenius plots. These are based on the Arrhenius relationship of eq 7, where $1/\tau$ is the relaxation rate (τ is the relaxation time), $1/\tau_0$ is the preexponential factor, U_{eff} is the effective relaxation barrier, and k is the Boltzmann constant.

$$1/\tau = 1/\tau_0 \exp(-U_{eff}/kT) \tag{7}$$

The obtained Arrhenius plots for **1** and **5** are given in Figure 14a,b, respectively. The fit of the data to eq 7 gave $U_{eff} = 50.1$ K, $1/\tau_0 = 3.61 \times 10^8$ s⁻¹ for **1** and $U_{eff} = 55.1$ K, $1/\tau_0 = 1.30 \times 10^9$ s⁻¹ for **5**. Note that the $U_{eff} = 50.1$ K value refers to the slower relaxing form of **1** in the wet crystals (see Figure 11), whereas the magnetization fits and the in-phase ac susceptibility data leading to the conclusion that $S = 6$ were for the dried solid, which is almost all the faster relaxing form (see Figures 11 and 12).

Hysteresis Studies below 1.8 K. The observation of out-of-phase ac signals suggested that **1** and **5** might be new SMMs, although such signals by themselves are not proof of an SMM. To confirm whether **1a,b** and **5·6CH₂Cl₂** are indeed SMMs, magnetization vs dc field sweeps were performed on single crystals of **1a,b** and **5** using a micro-SQUID apparatus.[18] These studies also allowed assessment of the differences in the magnetic properties of the two crystal

(a)

(b)
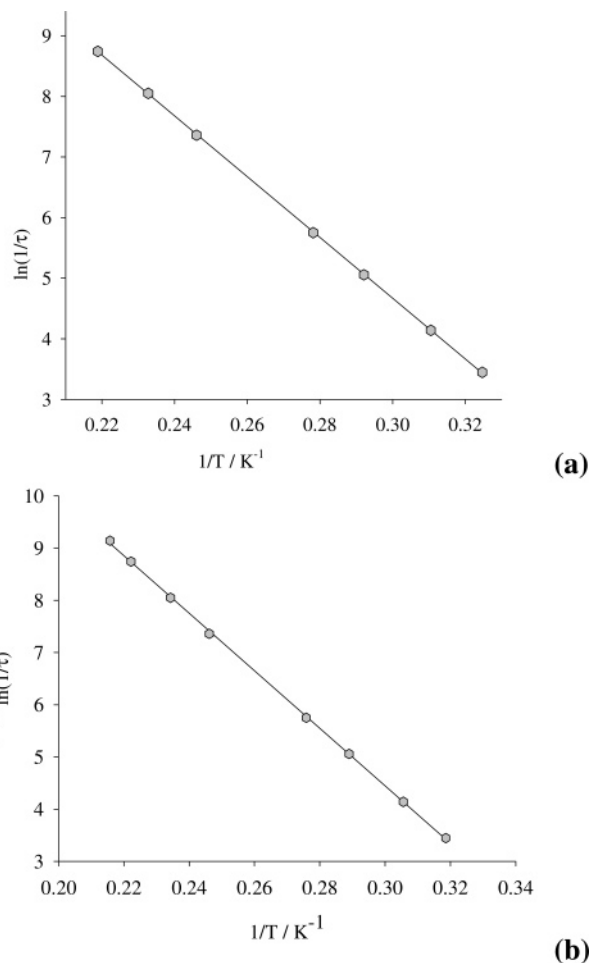
**Figure 14.** (a) Plot of the natural logarithm of relaxation rate, $\ln(1/\tau)$, versus inverse temperature using the χ_m'' vs T data for the slower relaxing species (higher temperature data) from a wet microcrystalline sample of complex **1**. (b) Plot of the natural logarithm of relaxation rate, $\ln(1/\tau)$, versus inverse temperature using the χ_m'' vs T data for the slower relaxing species (higher temperature data) from a wet microcrystalline sample of complex **5·6CH₂Cl₂**. The solid line is a fit to the Arrhenius equation; see the text for the fitting parameters.

forms of **1**. The obtained results are shown in Figures 15 and 16, which confirm that both crystal forms exhibit magnetization hysteresis and are thus SMMs. The variable-temperature data for complexes **1a,b** at a 0.017 T/s sweep rate are shown in Figure 15 (top and bottom, respectively), and they can be seen to be overall very similar. In both cases, the coercivities (half the loop width at $M/M_S = 0$) increase with decreasing T, as expected for the superparamagnet-like properties of a SMM. The variable-sweep-rate data for complexes **1a,b** are shown in Figure 16 (top and bottom, respectively) at a constant temperature of 0.04 K, and the coercivities can be seen to increase with increasing sweep rate, again as expected for a SMM. In all cases, the dominating feature is a large step at zero field due to quantum tunneling of the magnetization (QTM) through the anisotropy barrier. This provides another route for magnetization relaxation, and the step thus represents a surge in the rate of reorientation of the magnetization vector.

An overall comparison of the hysteresis loops of **1a,b** reveals that they are extremely similar, nearly superimposable within experimental error. This is totally inconsistent with
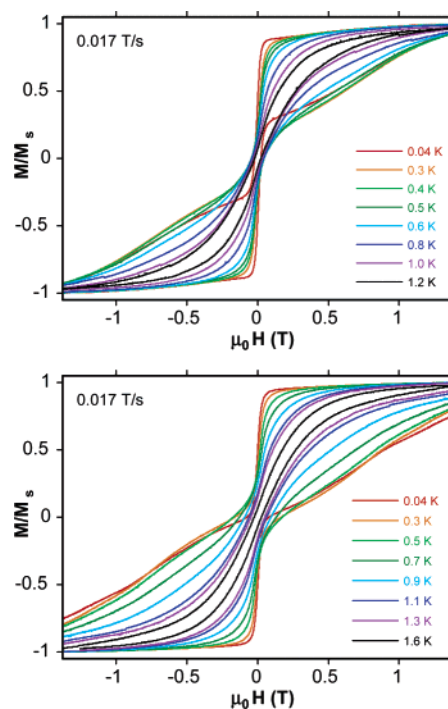
Figure 15. Magnetization (M) vs applied dc magnetic field ($\mu_0 H$) hysteresis loops at a 0.017 T/s sweep rate for a single crystal (wet with mother liquor) of **1a** (top) and **1b** (bottom) at the indicated temperatures. M is normalized to its saturation value, M_s.
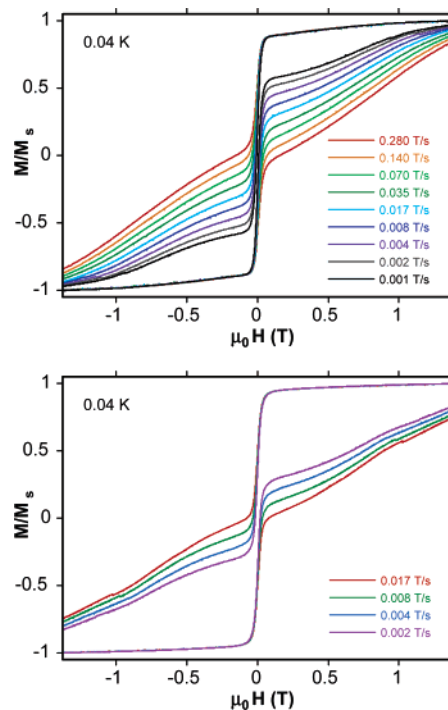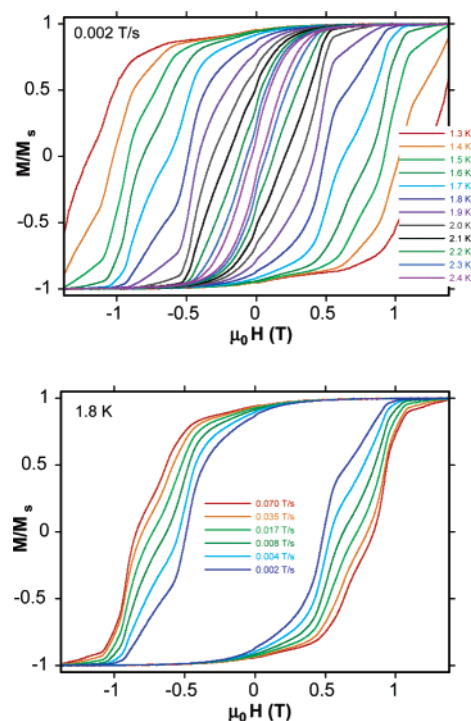

Figure 16. Magnetization (M) vs applied dc magnetic field ($\mu_0 H$) hysteresis loops at 0.04 K for a single crystal (wet with mother liquor) of **1a** (top) and **1b** (bottom) at the indicated field sweep rates. M is normalized to its saturation value, M_s. Avalanche problems were observed for **1b** at sweep rates faster than 0.017 T/s, and these sweeps have therefore been omitted.

the at-first-glance "logical" conclusion that the two crystal forms **1a,b** are responsible for the two ac signals in Figure 11. This would require the two crystal forms to have significantly greater differences in their relaxation rates (i.e.

their relaxation barriers), which would have resulted in distinctly different hysteresis profiles. We thus conclude that the two ac signals in Figure 11 are *not* due to the two crystal forms **1a,b**. However, a closer examination of the hysteresis loops for **1a,b** suggests that each crystal form is itself a mixture of two species: one of them is a faster relaxing species that is responsible for the large decrease in magnetization at zero field (i.e. for the large QTM step at zero field), and the other is responsible for the subsequent feature at higher fields due to a slower relaxing species. These two species now can reasonably be assigned as the two species responsible for the two ac signals in Figure 11: the slower relaxing species gives the frequency-dependent signal in the 3−4.5 K range (higher temperature, or HT signal), whereas the faster relaxing species gives the lower temperature (LT) signal at <1.8 K. The relative proportions of the features due to the slower (HT) and faster relaxing (LT) species in the hysteresis loops suggest comparable amounts of the LT and HT forms in each crystal, with perhaps a slightly greater amount of the former, and this is again consistent with the relative proportion of LT and HT ac signals in Figure 11. Note that the hysteresis and ac studies were performed on a wet single crystal in Apiezon grease and wet microcrystalline material suspended in solid eicosane, respectively, and thus under similar but not strictly speaking exactly the same conditions.

The remaining question is what causes the difference between the HT and LT forms in both **1a,b**? We believe that the answer is Jahn−Teller isomerism, a phenomenon already well established in normal Mn₁₂ chemistry. JT isomers are species that differ in the relative orientation of one or more Mn^{III} JT distortion axes, and these have been found to have distinctly different barriers to magnetization relaxation (by a factor of 2 or so) and thus to give ac signals at significantly different temperatures. The normal, slower relaxing JT isomers give ac signals at higher temperatures (HT form) and have all their Mn^{III} JT axes near-perpendicular to the Mn₁₂ disklike plane. In contrast, crystals of pure faster relaxing JT isomers (LT form) can be prepared with, for example, *tert*-butylacetate as the carboxylate group, and crystallography on these has identified the faster relaxing form to be due to the abnormal orientation of one (or more) Mn^{III} JT elongation axes, being disposed in the Mn₁₂ disklike plane and thus pointing to a core O²⁻ ion.[6d,g] We believe this is the origin of the two forms of **1**. Indeed, this takes us back full circle to the crystal structures described above, because it rationalizes the unusual Mn−O bond lengths at Mn4 for **1a** and Mn1 for **1b**. For **1a**, for example, an approximately equal mixture of (a) slower relaxing species with the JT axis at Mn4 in the normal position along the O9−Mn4−O14 axis and (b) faster relaxing species with the JT axis at Mn4 abnormally aligned along the O7−Mn4−O12 axis will lead to the crystallographic average result that the O9−Mn4−O14 and O7−Mn4−O12 bond lengths are shorter and longer, respectively, than they should be, which is what is seen. The situation is similar for Mn1 in **1b**. We thus feel that the crystallographic data support the conclusion from the magnetic studies that crystals of **1a,b** comprise a

Figure 17. Magnetization (*M*) vs applied magnetic field (*μ₀H*) hysteresis loops for a single crystal (wet with mother liquor) of **5**·6CH₂Cl₂ at (top) the indicated temperatures and a field sweep rate of 0.002 T/s and (bottom) the indicated field sweep rates and a constant temperature of 1.8 K. *M* is normalized to its saturation value, *M*ₛ.

mixture of slower and faster relaxing species resulting from normal and abnormal orientations, respectively, of a Mn^{III} JT elongation axis. As with normal Mn₁₂ complexes, it will require crystallization of pure crystals of the different forms of **1** to allow more detailed study, and this is a current objective.

Putting all the above together leads to the following conclusions about complex **1**: (i) The two crystal forms **1a,b** contain essentially identical [Mn₁₂O₁₂(OMe)₂(O₂CPh)₁₆-(H₂O)₂]²⁻ dianions. (ii) Each crystal form contains a co-crystallized mixture of faster relaxing (LT) and slower relaxing (HT) species that are JT isomers. (iii) The two HT forms and the two LT forms have practically indistinguishable magnetic properties, thus giving only one HT ac signal when a mixture of the forms was studied and exhibiting almost superimposable hysteresis loops when the crystals were studied separately. (iv) The differences in space group and the content of solvent molecules of crystallization in orthorhombic (NBuⁿ₄)₂[Mn₁₂O₁₂(OMe)₂(O₂CPh)₁₆(H₂O)₂]·2H₂O·4CH₂Cl₂ (**1a**) and triclinic (NBuⁿ₄)₂[Mn₁₂O₁₂(OMe)₂-(O₂CPh)₁₆(H₂O)₂]·2H₂O·CH₂Cl₂ (**1b**) have an indistinguishable effect on the resulting magnetic properties. and (v) Complex **1** is a new addition to the family of SMMs.

Finally, Figure 17 shows the hysteresis loops obtained for complex **5**·6CH₂Cl₂ at different temperatures and a field sweep rate of 0.002 T/s (top) and at different sweep rates at a constant temperature of 1.8 K (bottom). The coercivity increases with decreasing *T* and with increasing field sweep rate, as expected for a SMM. Thus, complex **5**·6CH₂Cl₂ is a SMM. This is as expected for salts of the one-electron-reduced form of the normal Mn₁₂ family.[6f,9]

Conclusions

In this paper, we have reported a new, reductive aggregation procedure to a number of polynuclear Mn complexes consisting of the reduction of permanganate by MeOH in the presence of carboxylic acid. The most interesting of the complexes described is **1**, a new structural type of mixed-valent Mn_{12} ($4Mn^{IV}$, $8Mn^{III}$) complex which is structurally similar to and at the same oxidation level as the well studied, normal Mn_{12} type but which contains a somewhat different core structure. Also unusual is the chain polymer **2**, a rare example of such a 1-D polymer in Mn^{III} carboxylate chemistry. This new reductive aggregation procedure promises to provide a rich new single-source route to a variety of high-nuclearity Mn products not accessible by the more common comproportionation procedures. For this reason, reductive aggregation reactions are being carried out under a variety of conditions, and further results will be reported in due course.

Supporting Information Available: X-ray crystallographic files in CIF format for complexes **1**·2H$_2$O·4CH$_2$Cl$_2$, **1**·2H$_2$O·CH$_2$Cl$_2$, **2**, **4**·2MeOH, and **5**·6CH$_2$Cl$_2$. This material is available free of charge via the Internet at http://pubs.acs.org.

IC050868W